# Weathering indices as climate proxies. A step forward based on Congo and SW African river muds

Pedro A. Dinis[1]*, Eduardo Garzanti[2], Annette Hahn[3], Pieter Vermeesch[4], Marina C. Pinto[5]

[1] MARE - Marine and Environmental Sciences Centre, Department of Earth Sciences, University of Coimbra, 3030- 790 Coimbra, Portugal

[2] Laboratory for Provenance Studies, Department of Earth and Environmental Sciences, University of Milano-Bicocca, 20126, Milano, Italy

[3] MARUM Center for Marine Environmental Sciences, University of Bremen, Bremen, Germany

[4] University College London, London, WC1E 6BT, UK

[5] Geobiotec Research Centre; Department of Geosciences of University of Aveiro, 3810-193 Aveiro, Portugal

* Corresponding author: pdinis@dct.uc.pt

**Abstract:** Despite the influence of other geological and geomorphological factors, chemical weathering at the Earth's surface is strongly controlled by climate. Thus, a measure of weathering intensity determined from soils or sediments should provide information about the climatic conditions associated with their formation. Available geochemical and mineralogical data on modern fluvial and marine muds from different regions of southern Africa and its Atlantic continental margin are used to review the links between sediment composition and climatic properties together with the possible causes of variance. Although river muds may not be generated exclusively in a single sedimentary cycle and erosion and weathering processes do not necessarily take place in a spatially homogeneous way, significant relationships between mineralogical and geochemical signatures of river mud and rainfall in the corresponding catchment area were recognised. Our study shows that the composition of clay is strongly influenced by climatically-driven weathering, whilst coarser mud fractions tend to be more affected by provenance, grain size, hydraulic sorting, and recycling. In the marine environment the climatic signal may be lost even in clay, because of hydraulic fractionation, authigenic mineral growth and mixing with foreign particles. Given the ubiquitous character of fluvial muds, and the easy and non-expensive methods available for separating and analysing clay fractions, their geochemical fingerprints represent a most precious source of information concerning climate. Any geochemical parameter used as a regional proxy of climate, however, still requires that the diversity of geological, geomorphological, and biological factors that affect its value are cautiously considered.

**Keywords:** Chemical weathering; Mud composition; Climate; SW African margin; Congo; Rainfall proxies

## 1. Introduction

Paleo-climate records from continental settings are crucial to test the performance of general circulation models and to understand forcing factors of different components of the climate system. The quest for climatic proxies has shown that isotope data determined in mammals' teeth and bones (Grimes et al., 2008; Bernard et al., 2009; Royer et al., 2013), speleothems (McDermott, 2004), fresh-water biota (Schmitz and Andreasson, 2001), vegetal remains (Diefendorf et al., 2010), authigenic lake sediments (Leng and Marshal, 2004) and other materials are able to provide robust information on local environmental conditions. However, speleothems are found only in very specific settings and the organic components are not always present or sufficiently well preserved in continental deposits to make accurate isotopic analysis.

Siliciclastic deposits can be regarded as excellent archives of past environmental conditions, and the composition of loess (e.g., Porter, 2001; Yang et al., 2004; Schatz et al., 2015) and fine-grained fluvial units (e.g., Dinis et al., 2017; Guo et al., 2018) are particularly suitable for climatic reconstructions. The postulated links between fluvial mud composition and climate are based on the fact that most fine-grained sediment carried in suspension is eroded soil derived from the source areas whose mineralogy and geochemistry, namely the levels of depletion in mobile elements relative to parent rocks, are largely dependent on weathering intensity (Viers et al., 2009). Furthermore, weathering rate has a crucial role in feedback mechanisms of the climate system (Walker et al., 1981; Berner et al., 1983), making its investigations particularly pertinent. A reliable climate proxy based on the geochemical and mineralogical composition of the widespread worldwide river mud deposits would thus allow a much broader understanding of past climatic conditions in continental settings. Unfortunately, the interpretation of the climatic control on the composition of muds is not a straightforward task. Mud geochemistry and mineralogy are controlled by many diverse factors (Singer, 1980; Fedo et al., 1995; Gaillardet et al., 1999; Thiry, 2000; Borges et al., 2008; Garzanti et al., 2011; von Eynatten, 2012, 2016) so that the role of climate is difficult to single out.

The present research arises from previous works focused on the weathering influence on the mineralogy and geochemistry of present-day river mud deposits from equatorial to sub-tropical southern Africa (Garzanti et al., 2013, 2014; Dinis et al., 2017). Complementing earlier approaches, we make use here of an extended set of river mud samples, include also marine muds collected offshore of the Congo river-mouth, and specifically consider geochemical data for the clay fraction. Ultimately, compositional data obtained for different silt and clay size fractions are tested as regional proxies of climatic variables. We also show how other exogenous factors may control mud composition and discuss opportunities to minimize biased climatic interpretations based on the composition of mud deposits.

## 2. The climate-weathering link

### 2.1 Weathering intensity versus weathering rate

Weathering rate reflects the rates of dissolution of bedrock by surficial fluids and removal of ions in solution and is usually expressed as the amount of mobilised material per units of area and time (von Blanckenburg et al., 2005). A review of the methods used to estimate weathering rates was presented by Minasny et al. (2015). The intensity of chemical weathering affecting a given region is frequently assessed through the composition of the produced soils or sediments using ratios of elements or sets of elements that respond differently to chemical decomposition of rock-forming minerals in exogenous environments. There is a global agreement that the intensity of weathering at the Earth's surface largely depends on climate, being higher in warmer and more humid settings. Several authors postulate that the rate of mineral decomposition at the watershed scale increases with temperature following the Arrhenius equation (Bradly and Carrol, 1994; White and Blum, 1995; Dessert et al., 2003). In this equation, temperature is a power variable responsible for doubling the rate of the reaction for each 10°C rise. In addition, the influence of temperature on weathering rates would be dependent on precipitation, being substantially higher in more humid watersheds (White and Blum, 1995).

However, there is no consensus about the effective role of climate on weathering rates. While some argue that temperature and precipitation/runoff exert a strong influence (White and Blum, 1995; West et al., 2002), others showed that the exposure of fresh material is probably the most important controlling factor (Huh and Edmond, 1999; Oliva et al., 2003). In either case, physical denudation rates must exert a fundamental control on weathering intensity (Riebe et al., 2004; West et al., 2005; Gabet and Mudd, 2009). In slowly eroding settings, surface sediment suffers intense decomposition before removal and the rate of weathering is limited by the supply of fresh material ("supply-limited" conditions). Where denudation is high, the rate of weathering tends to be limited by the kinetics of surface reactions, the so-called "weathering-limited" (Riebe et al., 2004) or "kinetic-limited" (West et al., 2005) conditions, and depends on the time available for weathering reactions and the kinetics of the reaction, which is controlled by temperature, water supply, and vegetation cover (West et al., 2005). A weak relationship between climatic variables and weathering rate can be detected, but just after removing the effects of physical denudations, which play a dominant role (Dupré et al., 2003; Riebe 2004; von Blanckenburg, 2005).

Weathering profiles are expected to be thicker and their upper levels more depleted in mobile elements in wetter and warmer environments, hence revealing higher weathering intensities. But a thick regolith cover will limit weathering rates because freshly exposed material tends to weather more rapidly than the old material that is already depleted in the most reactive components, thus explaining the high weathering rates in watersheds under strong denudation stress (Riebe et al., 2004; Gabet and Mudd, 2009) or in dry/cold settings influenced by mechanical break-down caused by frost action (Huh, 2003; Gabet et al., 2010). This is why, at a global scale, an increase in weathering rate is expected when frost action becomes effective and low rates occur in warm/humid regions with thick regolith sequences (Huh, 2003). As summarized by Humphreys and Wilkinson (2007), soil production may either decrease exponentially with soil thickness or reach maximum at a certain soil thickness, but is invariably low in regions with thick regolith cover. High soil production in areas under rapid denudation that tend to have thin regoliths accounts for the inverse relation between suspended load and weathering intensity in big rivers (Gaillardet et al, 1999). From the previous discussion it is clear that weathering rates and weathering intensities respond to climate differently. Only a tangible property influenced by climate and measured from weathering products can be used to approximate paleoclimatic conditions.

## 2.2 Proxies of weathering intensity

The intensity of chemical weathering affecting a specific region can be estimated through diverse compositional indices applied to soils and sedimentary deposits (Table 1). Since the definition of the Weathering Index of Parker (WIP; Parker, 1970) and, in particular, of the Chemical Index of Alteration (CIA; Nesbitt and Young, 1982), the chemical composition of siliciclastic sediments has been widely used to infer paleoclimate (e.g., Kalm et al., 1996; Ehrmann, 1998; Hodell et al., 1999; Hong et al., 2007; Liu et al., 2014; Clift et al., 2014; Hessler et al., 2017). The CIA is probably the most popular geochemical weathering index, although others are commonly used as well, namely the Chemical Index of Weathering (CIW; Harnois, 1988), the Plagioclase Index of Alteration (PIA; Fedo et al., 1995), the Chemical Proxy of Alteration (CPA; Buggle et al., 2011) and the modified CIA index (CIX; Garzanti et al., 2014). Overviews of the rationale of these weathering indices were presented in previous studies (Price and Veldel, 2003; Sheldon and Tabor, 2009; Guo et al., 2018). The alternatives to CIA were proposed to overcome recognised drawbacks on its application, such as the non-consistent behaviour of K during weathering (Harnois, 1988; Maynard, 1992), the occurrence of K-metasomatism/illitization (Fedo et al., 1995; Buggle et al., 2011), and the difficulties in establishing carbonate bound CaO (Buggle et al., 2011; Garzanti and Resentini, 2016). All of these parameters estimate weathering intensity based on the molar proportions of silicate-bound major elements. Excepting the WIP, where the value of the index is proportional to the concentration of mobile elements, they rely on a ratio between the non-mobile element Al ($Al_2O_3$ minus $K_2O$ in PIA) and a set of non-mobile components that tend to be leached out during feldspar decomposition. Hence the value of the index tends to increase with weathering intensity.

Because most of these compositional parameters provide no information about the fate of Fe and Mg (only WIP considers Mg), which are preferentially hosted in olivine, amphibole, and pyroxene, other procedures were proposed to estimate weathering intensity affecting source rocks with these elements. The Mafic Index of Alteration ($MIA_{(o)}$ and $MIA_{(r)}$; Babechuck et al., 2014) is defined in a similar way as the CIA, but includes Fe in the group of mobile elements if the environment is reduced or added to Al in an oxidative environment. Additional multi-element approaches were also proposed. Using a Principal Component Analysis (PCA) applied to igneous rocks and their weathering products, Ohta and Arai (2007) defined a Mafic-Felsic-Weathering ternary diagram (MFW) in which the values for each vertex are obtained through mathematical expressions based on the weight percentage of major elements ($SiO_2$, $Al_2O_3$, $Fe_2O_3$, $TiO_2$, MgO, $K_2O$, $Na_2O$ and silicate-bound CaO). In that work, it was proposed that the way samples plot in the MFW diagram reflects both the relative contribution of mafic/felsic source rocks and the weathering intensity. The diagram $M^+$-4Si-$R^{2+}$ of Meunier et al. (2013) is also intended to tackle the problem of different source-rock composition and weathering intensity with a ternary diagram. In that article, composition is expressed as monocationic millimoles ($M^+=Na^++K^++2Ca^{2+}$; 4Si=Si/4; $R2^+=F^{2+}+Mg^{2+}$). Sediments derived from felsic to ultra-mafic rocks appear in different fields parallel to the M+-R2+ border, and weathering intensity progresses towards the kaolinite pole represented by the 4Si vertex.

Many other ratios between two elements with different mobility were used as proxies of weathering intensity, including $K_2O/Al_2O_3$ and $Na_2O/Al_2O_3$ (Gallet et al., 1995), Th/U (Gu et al., 2002), Th/K (Deconinck et al., 2003), K/Na and Rb/Sr (Yang et al., 2004), Cs/Ti and Rb/Ti (Yan et al., 2007), and Rb/K (Roy et al., 2008). These ratios are not applicable for instance where the value is lower than in the UCC (Upper Continental Crust) standard (e.g., Th/U), or where chemical decomposition is too strong (e.g., K/Na and Rb/Sr) or too weak (e.g., $K_2O/Al_2O_3$, $K_2O$/Th, Rb/K). Gaillardet et al. (1999) defined alfa ($\alpha_E$) weathering indices for different mobile elements by comparing their concentrations with that of a non-mobile element with similar magmatic compatibility in the sample and in the Upper Continental Crust (UCC) standard. Alfa indices were thus defined as the ratio between a non-mobile and a mobile element normalised by the same ratio in the UCC (e.g., $\alpha_{Mg}=[Al/Mg]_{sample}/[Al/Mg]_{UCC}$; $\alpha_{Na}=[Sm/Na]_{sample}/[Sm/Na]_{UCC}$). With the exception of Al, the suggested non-mobile elements (Ti, Th, Sm and Nd) are strongly affected by the sorting processes that control heavy-mineral concentration (Garzanti et al., 2009). Hence, to avoid the bias introduced by hydraulic sorting, Garzanti et al. (2013) suggested referring all elements to Al ($\alpha^{Al}{}_E$), which is hosted in minerals with different density (e.g. feldspar and garnet) and shape (e.g., tectosilicates and phyllosilicates) and is thus much less markedly influenced by hydraulic-sorting processes. When dealing with source areas that are not akin to the UCC, such as volcanic islands or continental flood basalts, different appropriate reference materials (e.g., average composition of volcanic or plutonic source rocks) should be used to establish the levels of depletion (Garzanti et al., 2013; Dinis et al., 2019).

Since the mid-20th century, also clay mineralogy is widely used as a tracer of paleoclimate (Klingebiel, 1963; Sittler and Millot, 1964; Power, 1969; Bierkland, 1969).

The assumption that clay assemblages reflect coeval climate conditions is supported by the long known distribution of clay minerals around the world's oceans, which largely reflects climate and weathering intensity in adjacent continental areas (Biscaye, 1965; Griffin et al., 1968). For example, kaolinite is abundant in wet areas where chemical decomposition is intense, smectite is common in warm regions with a well-defined dry season characterized by intense evaporation, and illite and chlorite dominate where erosion is chiefly physical and decomposition is minor (Chamley, 1989; Velde, 1996). A discussion on the weakness of clay assemblages as proxies of weathering intensity is presented below. Other authors used a Mineralogical Index of Alteration (MIA) based on the proportions of quartz and feldspar (Rieu et al., 2007; Hessler et al., 2017). The proportion of these minerals, however, largely depends on sediment grain-size, hampering the application of such index in interpretation of climate-driven weathering (Garzanti et al., 2019).

## 3. Congo and southwest Africa case-study

Southwest Africa has excellent conditions to review the links between sediment composition, weathering intensity and climate. This vast region is characterized by a stark contrast in climatic conditions (Fig, 1), and also the other factors that affect mud composition are spatially variable, namely physiography (e.g., slope, size of drainage basins, elevation of flat and steep areas, relationships between topography and climatic variables) and geology (e.g., crystalline rocks of different composition, lava fields, proportion of multicycle sedimentary successions; Fig. 2; Appendix A).

## 3.1. Geology and geomorphology

### 3.1.1. Atlantic margin

Several Cretaceous and Cenozoic stages of uplift affected the western margin of southern Africa after initial opening of the South Atlantic Ocean (Burke and Gunnell, 2008; Guillocheau et al., 2018). These tectonic processes, which controlled the development of Meso-Cenozoic sedimentary basins and the configuration of the drainage network, are most prominent in southern locations where more than 4000 m of crustal uplift is estimated (Jackson et al., 2005; Guiraud et al., 2010). Along the Atlantic margin of the Democratic Republic of Congo (DRC) and Angola, an Upper Cretaceous to Holocene sedimentary succession reaching several km in thickness is widely exposed in onshore areas of the Lower Congo (~85 km), Kwanza (~ 135 km), and Namibe (~50 km) basins (e.g., Moulin et al., 2010; Chaboureau et al., 2013 and references herein). The succession starts with coarse-grained alluvial deposits that are followed by thick evaporites and diverse marine or coastal siliciclastic and carbonate units (Guiraud et al., 2010). This continental margin is mainly volcanic-poor (Contrucci et al., 2004; Séranne and Anka, 2005), although Lower Cretaceous syn-rift mafic volcanic rocks occur (Marzoli et al., 1999).

The basement includes Archean rocks of the Congo craton and bordering Proterozoic orogenic belts associated with the amalgamation of West Gondwana (Basei et al., 2008; Heilborn et al., 2008; Vaughan and Pankhurst, 2008). At lower latitudes (<10°S), Meso-Cenozoic strata non-conformably overlie Paleoproterozoic crystalline units (Kimezian; ~2 Ga) that define a < 100 km-wide elongated ribbon to the west of the Neoproterozoic

West Congo Belt. The West Congo Supergroup is represented by a mainly Tonian volcano-sedimentary succession that shows eastward-decreasing deformation and metamorphic grade and is covered by Cryogenian to Ediacaran siliciclastic and carbonate strata (Tack et al., 2001; Kadima et al., 2011). Basement geology changes south of ~10° S, where the Congo craton is mostly represented by Eburnean (~2 Ga) granitoids of the Angola Block (de Waele et al., 2008). The Angola Block also includes Neoarchean granitoids, high-grade metamorphic rocks, and mafic complexes at its north-eastern edge (Carvalho et al., 2000), and large mafic intrusions of the Mesoproterozoic Cunene Intrusive Complex at its south-eastern edge (Carvalho et al., 2000; Mayer et al., 2004; Becker et al., 2006). A poly-orogenic complex with reworked Precambrian crystalline rocks is exposed to the west and reaches~150 km in width in southern sectors.

More than 200 km from the coastline, occurs the mainly Cenozoic, sand-dominated fluvial and aeolian succession of the Kalahari Basin (Wiggs et al., 1995; Haddon and McCarthy, 2005). The Kalahari succession is preserved in a relatively continuous subsiding area between the Republic of South Africa and the DRC, although with discrete depocenters that started to form during the Late Cretaceous or Early Cenozoic following uplift of southern African margins (Haddon and McCarthy, 2005).

### 3.1.2. Congo river basin

With a catchment area of ~3.7 million km$^2$ and 4200 km-long, the Congo is one of the largest rivers in the world, draining most of the DRC as well as significant parts of the Central African Republic, Angola, Zambia, and Tanzania. In central position, a broadly circular intracratonic basin 1000-1300 km in diameter (Congo Basin or *Cuvette Centrale*) coincides with a pronounced negative long-wavelength gravimetric anomaly (Crosby et al., 2010). The Congo Basin is an old subsiding continental area bounded by topographic highs that started to develop during the Late Proterozoic, probably in relation with failed-rift processes, and presents a thick sedimentary fill (up to 9 km) ranging in age from the late Neoproterozoic to the Holocene (Daily et al., 1992; Kadima et al., 2011).

The Congo Basin fill, thicker in a central area dominated by Cenozoic sediments, becomes thinner towards the margins where older units are exposed. Jurassic to upper Paleozoic outcrops only occur along its eastern flank (Daily et al., 1992; Giresse, 2005; Férnandez et al., 2015). Five major sequences were identified by Daly et al. (1992), whilst Kadima et al. (2011) considered three seismo-stratigraphic units separated by basin-wide unconformities. Meso-Cenozoic strata, making sequence 5 of Daly et al. (1992) and seismo-straigraphic unit C of Kadima et al. (2011), crop out in wide areas of the Congo Basin. The Cenozoic is well represented in the southern sector by Paleogene-Neogene deposits of the Kalahari Supergroup and by Plio-Pleistocene alluvial units in the basin centre (Fernandez-Alonso et al., 2015). These sediments were deposited when the borders of the *Cuvette Centrale* were uplifted, hampering marine incursions (Giresse, 2005). Cretaceous outcrops are most extensive along its southern edge, but occur also in numerous valleys along the eastern and northern margins of the *Cuvette Centrale*. Upper Jurassic and Upper Triassic strata are exposed along the banks of the Congo River and its tributaries in the eastern part of the basin (Fernandez-Alonso et al., 2015). Although Jurassic-Cretaceous strata are mainly continental, occasional marine incursions cannot be ruled out (Giresse, 2005). Older middle to upper Paleozoic redbeds, black shales, diamictites, along with other mudrocks and sandstone-dominated strata (seismo-stratigraphic unit B of Kadima et al, 2011; sequences 3 and 4 of Daly et al, 1992) are common along the eastern edge of the basin.

The oldest seismo-stratigraphic unit, Neoproterozoic to early Paleozoic in age (sequences 1 and 2 of Daly et al., 1992) are exposed in three major bordering regions of the Congo Basin, making the Cataractes and Inkisi Groups along the western margin of the basin, the Lindi Supergroup to the N and NE, and the Katanga Supergroup to the SE (Fig. 2). They consist of diverse siliciclastic and carbonate rocks, including stromatolitic and evaporitic sequences deposited in marine to lagoonal environments, followed by clastic deposits (Daly et al, 1992; Kadima et al., 2011). The Precambrian basement crops out in the elevated massifs that surround the Congo Basin. Archean cratonic cores are found in the Chailu-Gabon block to the west, in the Kasai block to the south, in the North-East Congo block to the NE, and in the Tanzania craton to the east. These massifs are separated by domains with mainly Paleoproterozoic (Eburnean) and Mesoproterozoic crystalline units, and by Pan-African orogenic belts (Fig. 2).

### 3.2. Climate in SW Africa

In SW Africa, a pronounced climatic gradient is marked by a continuous increase in rainfall from hyperarid Namibia and southern Angola to hyperhumid Congo. An oceanward decrease in humidity, usually restricted to the westernmost 200-300 km of the Atlantic margin, is recognised south of 2°S, whereas high rainfall occurs in coastal areas to the north (Fig. 1B). Unlike rainfall, average annual temperatures do not vary significantly, ranging between 20 and 30°C. Lower average temperatures occur only in the most elevated highlands near the eastern and southern borders of the Congo drainage basin and in coastal mountains of Angola. Given these patterns of variation of rainfall and temperature, climate is equatorial at lower latitudes, ranging from desert near the coastline to humid subtropical or temperate-highland tropical with dry winters in inner locations of higher latitudes (Peel et al., 2007).

Extending in latitude between ~9° N and 14° N, the Congo drainage basin is almost entirely situated in the subequatorial zone of high rainfall and temperature. Annual rainfall, with the exception of some eastern and southern marginal areas, is invariably higher than 1000 mm and reaches more than 2000 mm in wide lower-latitude sectors. The warm Angola Current explains the higher coastal humidity in equatorial and sub-equatorial areas, contrasting with southern coastal regions where aridity is linked with the Benguela upwelling system (Gordon and Bosley, 1991; Wacongne and Piton, 1992; Stramma and Schott, 1999). The intensity of the two currents and the position of their convergence zone are seasonally variable (Shannon and Nelson, 1996; Kostianoy and Lutjeharms, 1999; Hardman-Mountford et al., 2003). With the exception of the year-round humid equatorial region and the dry coastal fringe to the south, regional climates are usually characterized by alternating wet and dry seasons varying with latitude and distance from the coastline under the influence of the African monsoon system.

## 4. Methods

Twenty catchment areas from southwestern Africa with diverse geology and climate were selected for this study (Table 2). A Digital Elevation Model based on a Shuttle Radar Topography Mission (SRTM; spatial resolution of ~30 m) was applied to perform the delimitation of the catchment areas that drain to the sampling points using the

Hydrology tool package of ArcGIS 10. ArcGIS tools were also adopted for the quantification of the outcrop areas of the main geological units in each drainage basin and for the analysis of the spatial distribution of temperature and rainfall. Climatic variables were downloaded from WorldClim version 2 (http://www.worldclim.org/; Fick and Hijmans, 2017).

Twenty-two river mud samples, one for each catchment area, except for the Congo River with three samples collected in the lower Congo course, were investigated in more detail. The geochemical composition of these samples was determined for the grain-size fractions <32 µm and <2 µm, obtained from split aliquots by wet sieving and by centrifugation according to Stokes' law, respectively. Major oxides were determined by ICP-AES (using a Spectro Ciros/Arcos equipment) and trace elements by ICP-MS (using an ICPMS ELAN 9000 equipment) at Bureau Veritas laboratories (Vancouver). For further information on adopted procedures, geostandards used and precision see http://acmelab.com (group 4A-4B and code LF202). Element concentrations were compared to UCC composition (Rudnick and Gao, 2003; Hu and Gao 2008). For simplicity, Rare Earth Elements (REE) are grouped here as LREE (light REE; La, Ce, Pr, Nd and Sm), Eu, and HREE (heavy REE; Gd, Tb, Dy, Ho, Er, Tm, Yb and Lu). The mineralogy of the <2 µm fraction was determined by X-ray powder-diffraction (XRD) on oriented mounts, with a Philips® PW 3710 equipment with CuKα radiation using the software APD-PW1877 (version 3.6J). Diffractograms were obtained for air-dried mounts ($2\theta$ in the range 2-30°), and after treatment by ethylene glycol and heating to 550 °C ($2\theta$ in the range 2-15°). Mineral proportions were evaluated semi-quantitatively from diagnostic XRD peak areas, as estimated from intensity and width values, weighted by empirical factors using an in-house spreadsheet.

Muds collected offshore of the Congo river mouth during the Meteor cruises M6-6 (Wefer et al., 1988) and M20-2 (Schulz et al., 1992) were also investigated. For these samples, the sand fraction (> 63 µm) was removed via wet sieving and then the clay fraction (<5 µm) was separated by settling velocity, using Atterberg separation after Stokes' Law (Köhn, 1928). The elemental composition of each fraction was measured using a PANalytical Epsilon3-XL XRF spectrometer equipped with a rhodium tube, several filters and a SSD5 detector. Samples were dried and ground before measurements. A calibration based on certified standard materials (GBW07309, GBW07316, MAG-1) was applied to quantify elemental counts (c.f. Govin et al. 2014).

This dataset complements previously published results on mud composition of southern Africa. Namely for the clay mineralogy and the geochemistry of the <32µm fraction of SW African rivers (Garzanti et al., 2014; Dinis et al., 2017); for the clay mineralogy and the geochemistry of the<63m fraction of upper Congo rivers (Garzanti et al., 2013); and for the clay mineralogy of marine muds (Petschick et al., 1996).

## 5. Exogenous processes and mud composition

### 5.1. Levels of depletion and enrichment in different grain-size fractions

Significant depletions relative to the UCC were observed for Na, Ca, Mg, Si and K in the fractions <2 µm and <32 µm of the studied samples. Only the coarser fraction of a few mud samples collected in small rivers of the higher-latitude Atlantic margin show $K_2O$ content comparable or slightly higher than the UCC. The <32 µm fraction is invariably enriched in $TiO_2$ and Eu relative to the UCC. The other elements can be either depleted or enriched in both fractions (Fig. 3). Intersample compositional variability is particularly high for those elements most depleted relative to the UCC (Na and Ca), but significant variability is observed also for a few elements that are frequently enriched relative to the UCC (e.g., light REE, Nb). Silica, $Al_2O_3$ and $TiO_2$ display the lowest variability.

Considering intrasample compositional variability, the <2 μm fraction tends to be enriched in Al, Fe, Rb, Sc and V, and strongly depleted in Zr, Hf, Na and Ca relative to the <32 μm fraction. (Fig. 3A). The Mucope sample, which is entirely fed by recycled sediments from the Kalahari Basin, is a notable exception yielding higher Na and Ca and lower Rb in the <2 μm fraction. The concentration of other elements can be higher in either fraction, being usually approximately the same for Mg, REE, Y, and Nb. The concentration of Si and Ti also tends to be higher in the <32 μm fraction.

Joint statistical analysis of selected geochemical parameters ($SiO_2$, $Al_2O_3$, $Fe_2O_3$, MgO, CaO, $Na_2O$, $K_2O$, $TiO_2$, $P_2O_5$, MnO, Cs, Ba, Sc, LREE, HREE, Th, U, Zr, Nb, W and Co) was carried out by Principal Component Analysis (PCA) and visualised as compositional biplots (Fig. 4; Aitchison and Greenacre, 2002). The PCA configuration of the samples strongly suggests that weathering has a major effect on sediment composition, with river muds from wet (low latitude) and dry (high latitude) climates plotting at opposite ends of the biplots. The genetic reasons for the observed latitudinal trends are revealed by the vector loadings (arrows) of the biplot.

For the <32 μm fraction (Fig. 4A), the end points of the arrows define two directions (or 'links', Aitchison and Greenacre, 2002). The first link runs diagonally across the biplot and parallel to the aforementioned latitudinal trend. It connects the mobile elements

Ca and Na in the lower left corner to the immobile elements Al and Ti in the upper right corner. The second link runs perpendicular to the first one and connects elements that are compatible with mafic minerals (Co, Mn and Mg, upper left corner) with elements that are enriched in felsic minerals (U, Th, lower right corner). This trend suggests that the second link is controlled by sediment provenance. For the <2 µm fraction (Fig. 4B), the links are less clearly defined. Although the weathering trend is still clearly visible in the sample configuration, the provenance trend is less obvious. This supports the notion that the composition of the clay fraction is largely determined by weathering processes, which have erased most pre-existing provenance signature.

In order to better compare the levels of depletion or enrichment in different elements in the two fractions, a concentration factor $\alpha^{Al}_{E}$ (see section 2.2) was calculated for all elements. A ratio close to 1 means that the concentration of element *E* relative to non-mobile Al is comparable to that of the UCC. Substantially higher values indicate depletion, which can be ascribed to weathering; lower values indicate enrichment.As a direct consequence of phyllosilicate concentration in finer fractions, the Si/Al ratio notoriously reflects grain-size. Thus, the values of $\alpha^{Al}_{E}$ measured for most mobile elements tend to be higher in the <2 µm fraction, where Al-rich clay minerals are concentrated. Non-mobile elements such as Sc, Y, REE, Ti, Nb tend to be relatively enriched during weathering and hence frequently show $\alpha^{Al}_{E}$ values <1. As already shown elsewhere (Dupré et al., 1996; Gaillardet et al., 1999; Viers et al., 2009; Garzanti et al., 2013, 2014), Na is generally the most mobile element. For the <2 µm fraction, Na ($6.8 < \alpha^{Al}_{Na} < 201$) is far more depleted than all other mobile elements, namely Ca ($3.0 < \alpha^{Al}_{Ca} < 22$), Sr ($1.8 < \alpha^{Al}_{Sr} < 19$), K ($1.6 < \alpha^{Al}_{K} < 5.7$) and Mg ($1.4 < \alpha^{Al}_{Mg} < 5.4$). In muds, Th, U, LREE and Fe are the most enriched elements relative to the UCC. $TiO_2$, HREE, Y and Nb also tend to yield $\alpha^{Al}_{E}$ values <1 in the <32 µm fraction.

The high variability in concentration factors determined for some of the most mobile elements, such as Na and Ca, can be interpreted as evidence of strong weathering influence (Viers et al., 2009). A positive correlation between $\alpha^{Al}_{E}$ values in the two size-fractions is expected, whereas the poor correlation among elements such as Ti, Zr, Hf and Y hosted preferentially in the densest minerals (Fig. 5B) can be largely ascribed to hydraulic-sorting processes. The influence of provenance coupled with hydraulic sorting is particularly evident for Zr (Fig. 5C). Factors $\alpha^{Al}_{Zr}$ in the two fractions of fluvial muds sampled in higher-latitude regions are similar, whereas in mid-latitude regions the levels of depletion are notably lower for the <32 µm fraction. This may be ascribed to the presence of zircon grains sourced from the felsic-rich Eburnean massifs.

The geochemistry of marine sediments seems to be affected by sorting processes even more than river muds. The <5 µm fraction displays a clear increase in the Si/Al ratio and a decrease in Ti and Zr contents with water depth (Fig. 6). Precipitation of authigenic minerals (e.g., glaucony and carbonates) have a major effect on the levels of depletion/enrichment of different elements. Moreover, in marine settings far from fluvial entry points and in deep water the mixing of sediments transported from distant areas may overprint and blur the climatic signal hold by the mud sourced from adjacent continental areas, as observed for sands offshore of the Congo mouth (Garzanti et al., 2019).

### 5.2. Clay mineralogy evidence of weathering

The clay mineralogy of most fluvial mud samples considered here was presented in previous works (Garzanti et al., 2013, 2014; Dinis et al., 2017). Six newly analysed samples from the Congo drainage basin yielded mostly kaolinite with minor amounts of mica-illite. Two newly analysed samples from the Cunene drainage basin are enriched in smectite with subordinate amounts of kaolinite, quartz, and mica. The entire dataset (Fig. 7) confirms the trends for decreasing kaolinite with latitude, which reflects a decrease in humidity and weathering intensity (Chamley, 1989; Velde, 1995). Expansive clays (smectite and smectite-illite mixed layers) are more abundant at middle and high latitudes, where seasonally contrasted climatic conditions characterized by a dry period of intense evaporation generally occurs, and particularly so where mafic rocks are exposed in catchment areas. Relatively high mica-illite contents in some river-mud samples is attributed to the combined effects of feldspar weathering and disintegration of micaceous minerals inherited from source rocks (Dinis et al., 2017).

Offshore sediments of the southeastern Atlantic are kaolinite-rich at low equatorial latitudes, higher in smectite at middle latitudes (~10-20°) and in illite at higher latitudes (Petschick et al., 1996). In general, the ratio between kaolinite and mica+chlorite of marine samples from SW Africa is similar to that in river muds collected at comparable latitude (Fig. 7A), suggesting major control by river supply from adjacent continental areas. Smectite content, however, tends to increase with water depth. This is particularly evident for sediment collected offshore of the Congo River mouth, but it is also apparent in higher-latitude regions, lacking only at middle-latitude where fluvial and coastal muds are commonly smectite-rich (Fig. 7B and 7C). Selective settling of kaolinite, illite and chlorite, all generally coarser than smectite (Gibbs, 1977; Chamley, 1989; Petschick et al., 1996; Šimkevičius et al., 2003) may account for the observed basinward trend. Authigenic growth in marine environments is another possible cause for smectite enrichment (Cole and Shaw, 1983; Parra et al., 1985), and an association to the degradation of tephra ejected from volcanic centres of the Cameroon Line to the north was recently proposed for mud deposited on the continental slope and rise offshore of the Congo mouth (Garzanti et al., 2019). As for sediment geochemistry, it must be kept in mind that also the clay assemblage is affected by mixing with material transported by wind and surface or deep currents from distant sources (Petschick et al., 1996).

## 6. Weathering indices as climatic proxies

### 6.1. Relation between weathering intensity and climate

Several compositional features of marine sediments, such as their clay-mineral assemblage (Biscaye, 1965; Griffin et al., 1968; Petschick et al., 1996) and element ratios (Govin et al., 2012), point to a close link with climatic conditions on adjacent continental areas. The possible relationships between compositional features of modern fluvial mud and climatic variables were tested by several authors. In suspended load of North American rivers, the concentration of non-mobile elements Al and Fe correlates with runoff and precipitation, whereas an opposite trend was found for Ca and Mg (Canfield, 1997). Other works showed correlation between climatic (or climatic-driven) variables and weathering indices. Namely, between temperature and $\alpha_{Na}$ or $\alpha_{K}$ for big world rivers

(Gaillardet et al., 1999), between runoff and CIA for Southeast Asia (Borges et al., 2008), and between rainfall and $\alpha^{Al}_{Na}$ in sand, $\alpha^{Al}_{Mg}$ in mud, and clay-mineral assemblages in SW Africa rivers (Dinis et al., 2017). These relationships are ascribed to higher weathering intensity in wetter settings, with consequent leaching of most mobile elements and concentration of non-mobile elements in the weathered residue. However, the scatter attributed to the effect of different geologic and geomorphologic features of the drainage areas on sediment composition is very high. Such a strong variability is not surprising, because source lithology influences both the composition of weathering products (e.g., von Eynatten et al., 2012, 2016; Garzanti and Resentini, 2016) and the rate of weathering reactions (e.g., Meybeck, 1987; Kump et al., 2000; Amiotte Suchez et al., 2003; Jansen et al., 2010). Besides geological and geomorphological factors that control sediment composition, a time-scale problem may be also present, because a specific weathering stage may needs many thousands of years to be reached, whereas the climatic record, in terms of measured average temperature and rainfall, refers to the present day only which may be notably different from past conditions.

The compositional data of mud deposits presented for the first time here can be coupled with the comparable datasets presented in Garzanti et al. (2013, 2014) and Dinis et al (2017) to better understand the relation between weathering intensity and climate in southern Africa. Besides the equatorial and sub-tropical Atlantic margin and Congo system presented here in more detail, our integrated sample set includes data on muds from the upper branches of the Congo River in southern Burundi, Rwanda, and Tanzania, from the Zambezi, Limpopo, Okavango and Orange fluvial systems, and from western Namibian rivers. Climate data provided by WorldClim version 2 (http://www.worldclim.org/; Fick and Hijmans, 2017) for SW Africa indicate that both rainfall and temperature display major spatial variability (Fig. 1). Considering the average values measured in the catchments under investigation in Congo and SW Africa, rainfall is clearly more variable than temperature (Table 1). Furthermore, the study region is never as cold as in the case studies where the weathering dependence on temperature following the Arrhenius law seems to be applicable (e.g., White and Blum, 1991). Probably reflecting the homogenously warmer conditions, no significant relations were detected between temperature and any compositional feature indicative of weathering intensity.

Conversely, spatially-averaged rainfall co-varies with several compositional features indicative of weathering intensity (Figs. 8 and 9). Considering only geochemical parameters characterizing the <32 µm fraction (51 samples; upper Congo muds not included because the analyses were performed on the <63 µm fraction), $\alpha^{Al}_{Mg}$ (r=0.70), $\alpha^{Al}_{Ca}$ (r=0.59), WIP (r=-0.58), CIA (r=0.56), $\alpha^{Al}_{Sr}$ (r=0.55), and CIX (r=0.54) reveal the most significant correlations with rainfall. It must be noted that these correlations become weaker, or are even lost, if specific climatic and geographic contexts are analysed separately (Fig. 8). As far as non-mobile elements are concerned, no significant correlation was observed within the entire dataset, but if only the Congo drainage basin and the Angolan Atlantic margin are considered, $\alpha^{Al}_{E}$ for some of these elements anti-correlate with rainfall (r=-0.73 for Ti; r=-0.65 for Zr). A reasonable positive correlation between the kaolinite proportion in the clay-mineral assemblage and rainfall is also observed for the entire equatorial to sub-tropical dataset (r=0.63 for 66 samples).

Regarding the geochemistry of the <2 µm fraction, the original data presented here indicate that average rainfall in the catchment area correlates positively with $\alpha^{Al}_{Mg}$

(r=0.69), CIA (r=0.61), and $\alpha^{Al}_{Sr}$ (r=0.58). Because of quartz dominance in the wettest settings, the link between rainfall and the WIP is much weaker than in the <32 μm fraction, and the weakest among all of the other multi-element weathering indices. The highest negative correlation is found for $\alpha^{Al}_{Cs}$ (r=-0.57).

### 6.2. Spurious covariance of compositional features and rainfall

As shown by Garzanti and Resentini (2016), the values obtained for weathering indices may be largely determined by source-area lithology. In southern Africa, some co-variances between measured element abundances and rainfall are in fact influenced by geological processes not directly related to current rainfall. One evident case is the abundance of Ca and other mobile elements incorporated in carbonate minerals, which are expected to be higher where carbonate rocks are exposed. High Ca, Mg, and Sr actually occur in coarser mud fractions of southern rivers that drain Meso-Cenozoic basins of the Atlantic Margin characterized by moderately dry to very dry conditions or hinterland areas prone to pedogenic carbonate precipitation within the Kunene and Okawango river systems (Caculuvar and Kwando muds). Sorting processes also seem to have a major effect on the abundances of non-mobile elements in coarser mud fractions, as suggested before for Zr and Ti, among other elements preferentially hosted in heavy minerals (Fig. 5). Hence, provenance and sorting processes can exert a major influence on silt composition, leading to spurious correlations with rainfall. They may have forged apparent relations between the concentration of mobile/non-mobile elements and rainfall that are not necessarily linked with present-day climatically-driven chemical decomposition.

## 6.3 Focus on clay

Sediment composition is strongly influenced by the grain-size effect (von Eynatten et al., 2012, 2016). Because mud deposits may contain different proportions of clay and silt, even an analysis focused on mud may lead to biased interpretations of climate conditions. A closer relationship between clay mineralogy and chemical weathering than for the geochemistry of muds comprising silt fractions was already testified by Angolan Atlantic margin sediments (Dinis et al., 2017). In that research, however, the geochemistry of clay was not investigated, and mineral abundances estimated by XRD are not accurate (Moore and Reynolds, 1997; Kahle et al., 2002). For instance, a mixture in equal proportions of kaolinite, smectite and chlorite, three minerals indicating profoundly distinct climatic conditions, shows unequal (001) peak areas that depend on the chemical compositions of the minerals, their preferred orientation, and the structural arrangement of clay flakes.

More accurate results are expected to be obtained from geochemical analysis. Classical multi-elements weathering indices (e.g., CIA, CIX and CPA) and the $\alpha_E$ and $\alpha^{Al}_E$ indices used to establish element mobility are computed from ratios of the concentration of one or more mobile elements relative to a non-mobile element. . The concentration of the elements considered in these indices depend on the mineralogy of the source rock (e.g., felsic *vs*. mafic), a dependence that is apparently attenuated in finer fractions (von Eynatten et al., 2012, 2016; Dinis et al., 2017). The depletion of mobile elements in finer fractions with formation of residues enriched in Al regardless of source-rock composition partially accounts for this attenuation trend. In addition, clay fractions are not equally influenced by sorting processes, and therefore more likely reflect weathering processes coeval with deposition (Guo et al., 2018). Given the minor influence of hydraulic fractionation on clay geochemistry, the originally defined mobility indices α of Gaillardet et al. (1999) may not be distorted by these processes as much as when applied to sediments made of coarser particles.

Not all weathering parameters obtained from geochemical analysis of the clay fraction can be considered as robust estimators of climatic variables. For instance, K abundance in clay may be strongly dependent on source-area geology (von Eynatten et al., 2012, 2016; Garzanti and Resentini, 2016), which necessarily influences all indices that consider K, such as CIA, WIP, CIX, $\alpha^{Th}_{K}$, or $\alpha^{Al}_{K}$. Other indices (e.g., CPA, $\alpha^{Al}_{Na}$ and $\alpha^{Sm}_{Na}$) rely on Na as the mobile element, which is generally quite scarce in the clay-mineral lattice. In SW African river muds, $Na_2O$ concentration is locally near the detection level of 0.01%, hence introducing a supplementary risk of biased interpretation. Magnesium does not suffer from these issues, because it is invariably present in significant amounts in clay fractions and, despite overt differences between clays produced from mafic and felsic rocks in cold settings (Louvat et al., 2008; von Eynatten et al., 2012), the divergence seems to be reduced as weathering progresses, being apparently minor in wet and warm settings (von Eynatten et al., 2016). This is confirmed by the fact that in our study $\alpha^{Al}_{Mg}$ resulted to be a slightly better estimator of rainfall than all other compositional parameters (Fig. 9).

### 6.4. Geological and geomorphological causes of scatter

This section focuses on those factors that are expected to have a specific effect on the composition of clay, processes influencing compositional variability of coarser fractions having been discussed above.

6.4.1. Supply from areas with different climate

While evaluating weathering in the source area of sediments, we must keep in mind that chemical processes generally do not take place in homogenous environmental conditions. In big drainage basins, sediment derived from the most distant realms tend to pass through successive phases of transient deposition in alluvial plains and the composition may be more influenced by processes taking place in more proximal sites. Sediment composition can be affected also by processes occurring outside the drainage basins, as observed within or close to arid and semiarid regions, where even a significant fraction of fine-grained deposits seems to be allochthonous and airborne, generated in regions of completely different climate rather than within the river basin itself. Significant amounts of far-travelled sands was recognised in SW Africa (Garzanti et al., 2018a, 2018b) and this is even more plausible for very fine-grained particles. A similar complication has been discussed for marine deposits above.

6.4.2. Recycling

Even if only sediments produced within the drainage basin are considered, a major and long-recognised problem is the possible inheritance of compositional features from older sedimentary rocks (e.g., Singer, 1980; Gaillardet et al., 1999; Borges et al., 2008;

Garzanti and Resentini, 2016). Therefore, in general weathering indices reflect chemical processes that were cumulated during multiple depositional cycles, rather than weathering-related transformations coeval with the depositional unit. This problem is particularly pertinent in large catchment areas such as that of the Congo River, that include wide exposures of units formed in diverse previous sedimentary cycles (Duprè et al., 1996; Gaillardet et al., 1999). Although different methods were proposed to address the effect of recycling on weathering indices (Gaillardet et al., 1999; Garzanti et al., 2013; Dinis et al., 2017; Guo et al., 2018), this remains an issue difficult to solve. Comparing the composition of daughter sediments with parent rocks is a plausible way to quantitatively assess weathering-driven transformations during the last depositional cycle (Chetelat et al., 2015; Dinis and Oliveira, 2016). However, it may be quite difficult to accurately evaluate an average source-rock composition in large catchment areas. Lithium-isotopes combined with selected element ratios were also used to quantify the contribution of inherited weathering products in the particulate matter of big rivers (Dellinger et al., 2014; Wang et al., 2015).

Whereas sand is largely the product of physical erosion, clay is chiefly the product of climatically-driven weathering, which explains their stronger depletion in mobile elements. However, sand may also show extreme depletion in mobile elements whenever the effect of chemical processes during weathering and recycling is cumulated through multiple sedimentary cycles. A long multicyclic history typically ends up in quartz-enrichment (Garzanti, 2017), which is the case of Congo River sand that only includes the most chemically durable minerals (Garzanti et al., 2019). Congo muds, however, yield relatively low silica (34-43% in the <2 μm fraction), which is leached in association to kaolinite formation, and are enriched in some of the least mobile elements (i.e., Al and Ti). Where weathering is not extreme, as in the intracratonic Kalahari Basin where quartz is present in the clay fraction, recycling may promote silica enrichment in river muds (up to 58% $SiO_2$ in the <2 µm fraction and up to 66% in the <32 µm fraction). Recycling thus affects the composition of coarse and fine particles differently.

Silt and clay particles in fluvial mud deposits are entrained in suspension and tend to concentrate at different channel depths during transport (Rouse, 1937; Vanoni, 2006). Finest-grained particles are kept in motion even in the lowlands when current velocity is slow and competence decrease, being more likely winnowed in hypopycnal plumes offshore of the river mouth. The finest particles are also the most easily transported by wind. Based on these considerations, we hypothesize that the amount of this finest component is preferentially lost during multiple sedimentary cycles. If this is true, then the clay component in a modern sediment would represent climatic conditions during the last cycle far better than coarser fractions, and a ratio of the same weathering index in different grain-size fractions (e.g., <2 µm *vs.* <32 µm) may be used to assess recycling effects. This possibility is supported by the relationship between a ratio calculated with the levels of depletion of the most mobile element (i.e., ratio of $\alpha^{Al}_{Na}$ for <2 µm *vs.* $\alpha^{Al}_{Na}$ for <32 µm) with the percentage of Meso-Cenozoic sedimentary units in source areas (Fig. 10). River muds with similar levels of Na-depletion in the two size fractions that do not follow this trend occur in arid to semi-arid settings where airborne particles are most likely present and in catchment areas including sedimentary rocks of the West Congo Belt. In both cases, sources of recycled material alternative to Meso-Cenozoic sedimentary successions occur. As for other parameters, however, the influence of grain-size and source-area geology on coarser mud fractions and the very low Na content in the clay fraction where weathering is intense limits the application of this ratio as an estimator of recycling component.

6.4.3. Other surface processes

The size and relief of the catchment also exert a significant influence on sediment composition (e.g., Weaver, 1989). In small and relatively steep catchments exposing different lithological units sediment composition is expected to mirror the composition of those source rocks that erode faster. In steep areas, chemical decomposition is frequently hampered by the rapidity of erosion processes (“weathering-limited regimes” of Riebe et al., 2004, and West et al, 2005) and weathering reactions should be incomplete. Conversely, because widely different climatic conditions are generally present in large rivers, the relationship between sediment composition and climatic parameters is more complex. In addition, sediment temporarily stored in alluvial plains can suffer additional decomposition (e.g., Johnsson and Meade, 1990). Several authors maintained that floodplains are likely sites of weathering reactions (Galy and France-Lanord, 1999; West et al., 2002; Moquet et al., 2011), although minor changes in suspended load after temporary deposition were also reported (Bouchez et al., 2012). Assessment of climatic conditions from mud composition may thus be more reliable when dealing with drainage basins of medium size. In the present case, if data from sediments carried by the huge Congo River and by the rivers with drainage areas smaller than 2000 $km^2$ are neglected, the correlation between rainfall and $\alpha^{Al}_{Mg}$ is in fact notably improved (Fig. 9). A larger dataset with more diversified geomorphological and climatic conditions is however required to understand how the size of the drainage may influence the investigated relationships.

Another factor that should be considered is that water available for weathering reactions at the Earth’s surface does not depend exclusively on rainfall, as it is also controlled by the proximity of the water table. Weathering rates strongly depend on fluid residence time and flow rate (Maher, 2010), and higher weathering intensities tend to be attained in permeable mediums (Weaver, 1989; Hundert et al., 2006). Finally, the fluxes of weathering-related elements and soil composition depend on the interactions with vegetation and nutrient cycling (Minasny et al., 2015). Magnesium, along with other mobile elements, is an important nutrient influenced by biogeochemical cycles (White and Bum, 1995; Rufyikiri et al., 2004; Sardans et al., 2008; Barré et al., 2009). The transfers promoted by plants’ activity are thus likely to be responsible for changes in inorganic element concentration in the upper levels of soil profiles, which are most promptly eroded to generate fine particles entrained as suspended load.

### 6.4.5. Post-depositional transformations

A detailed description of the compositional transformations during diagenesis falls out of the scope of the present manuscript, but it must be pointed out that they inevitably blur the climatic signal in sediments generated and deposited in any environment. Muds are vulnerable to post-depositional transformations that may affect all weathering indices discussed before. Several authors have discussed changes in clay mineral assemblages and element concentrations caused by authigenesis in marine settings (e.g., Weaver, 1989; Thiry, 2000; Rimstidt et al., 2017), which can be accomplished by processes of reverse-weathering that consume silica (Michalopoulos and Aller, 1995; Tréguer and De La Rocha, 2013). In continental settings, early diagenesis may promote the enrichment of some mobile elements in weathering profiles (Nesbit and Young, 1989), whereas depletion may occur where permeable beds in regoliths or sedimentary successions allow water circulation (Hundert et al., 2006). As diagenesis proceeds, the compositional transformations also continue and may eventually lead to the replacement of detrital kaolinite and smectite by others minerals with higher Si/Al ratios, such as illite (Boles and franks, 1979; Hower et al., 1979; Chermak and Rimstidt, 1990; Fedo et al., 1995).

## 7. Concluding remarks

Weathering intensity, which is largely influenced by climate, can be estimated from the geochemical and mineralogical composition of sediments. Thus, the relationships observed on the Earth surface today between sediment composition and climate may help us to assess past climatic conditions. A series of problems, however, arise whenever geochemical and mineralogical indices are used as climatic proxies. The composition of daughter sediments is controlled primarily by the composition of the parent rocks. Moreover, even where source-area geology is similar, sediment composition will strongly depend on the grain size of the generated sediments. Mineralogical and chemical composition of detritus may be strongly influenced by hydraulic-sorting processes, which control the distribution of minerals with different density and shape in different size fractions. Other elusive factors that may be difficult to cope with are the dependence on the geomorphology of the drainage basin (e.g., size of the catchment, variable hillslopes and yields from different parts of the basin, proximity of the phreatic level) and the widespread and commonly overwhelming contribution of detritus recycled from pre-existing sedimentary units.

Climatic conditions are poorly reflected in the mineralogical and chemical composition of coarse silt and sand. The clay fraction is far more promising because heterogeneities in particle size tend to be lower and they largely consist of material eroded from coeval soils, thus more faithfully reflecting the environmental conditions during the last depositional cycle. In addition, it appears that the composition of clay is somewhat less dependent on the felsic vs. mafic provenance than coarser detritus. Fairly robust relationships between clay geochemistry and rainfall were in fact obtained for southern African river muds. The clay fraction, however, may be more affected by other interfering factors, such as the presence of allochthonous airborne material, and the process of plant uptake of mineral nutrients. Links between mud composition and climatic properties are even more difficult to establish in the marine environment. Here, mineral segregation by grain-size, mixture with allochthonous sediment transported from distant continental or intraoceanic areas, and formation of authigenic minerals commonly have a major effect on clay composition.

Despite these difficulties, regional climatic proxies based on mud composition are not destined for the dustbin. Mud is found in great abundance in all fluvial deposits worldwide. Sampling mud deposits, separating their clay fraction and determining their geochemical and mineralogical composition are simple and non-expensive tasks. The main challenge is to isolate the role played by the number of sedimentological, geomorphological, and biological factors that influence mud composition besides climatically-driven weathering. This can be partially achieved with large datasets from distinct size-fractions that are affected differently by diverse controlling factors. Advances in these issues will improve the performance of mud composition as an independent tool capable of approximating past climatic conditions in continental settings.

## Acknowledgments

The present work was supported by the FCT (Portuguese National Board of Scientific Research) through the Strategic Program MARE- Marine and Environmental Sciences Centre (UID/MAR/04292/2013) and by Project MIUR – Dipartimenti di Eccellenza 2018–2022, Department of Earth and Environmental Sciences, University of Milano-Bicocca. Johannes Remhof, Lígia Almeida. Luís Perdiz, Patrícia Soares and Rafael Rodrigues helped with the GIS project for the study area. The manuscript benefited from insightful and constructive reviews by Giovanni Vezzoli and two anonymous referees.

## References

Aitchison, J., 1983. Principal component analysis of compositional data. Biometrika 70, 57-65.

Aitchison, J., 1986. The statistical analysis of compositional data. London, Chapman & Hall.

Aitchison, J., Greenacre, M., 2002. Biplots of compositional data. Journal of the Royal Statistical Society: Series C (Applied Statistics) 51, 375-392.

Amiotte Suchet, P., Probst, J.L., Ludwig, W., 2003. Worldwide distribution of continental rock lithology: Implications for the atmospheric/soil CO2 uptake by continental weathering and alkalinity river transport to the oceans. Global Biogeochemical Cycles, 17, https://doi.org/10.1029/2002GB001891.

Araújo, A.G. Perevalov, O.V., 1998. Carta de recursos minerais de Angola/Mineral resources map of Angola. Ministério de Geologia e Minas, Instituto Geológico de Angola.

Babechuk, M.G., Widdowson, M., Kamber, B.S., 2014. Quantifying chemical weathering intensity and trace element release from two contrasting basalt profiles, Deccan Traps, India. Chemical Geology 363, 56–75.

Barré, P., Berger, G., & Velde, B., 2009. How element translocation by plants may stabilize illitic clays in the surface of temperate soils. Geoderma 151, 22-30.

Basei, M.A.S., Frimmel, H.E., Nutman, A.P., Preciozzi, F., 2008. West Gondwana amalgamation based on detrital zircon ages from Neoproterozoic Ribeira and Dom Feliciano belts of South America and comparison with coeval sequences from SW Africa. Geological Society, London, Special Publications, 294, 239-256.

Becker, T., Schreiber, U., Kampunzu, A. B., Armstrong, R., 2006. Mesoproterozoic rocks of Namibia and their plate tectonic setting. Journal of African Earth Sciences 46, 112-140.

Bernard, A., Daux, V., Lécuyer, C., Brugal, J. P., Genty, D., Wainer, K., Gardien, V, Fourel, F, Jaubert, J., 2009. Pleistocene seasonal temperature variations recorded in the δ18O of Bison priscus teeth. Earth and Planetary Science Letters 283, 133-143.

Birkeland, P.W., 1969. Quaternary paleoclimatic implications of soil clay mineral distribution in a Sierra Nevada-Great Basin transect. The Journal of Geology 77, 289-302.

Biscaye, P.E., 1965. Mineralogy and sedimentation of recent deep-sea clay in the Atlantic Ocean and adjacent seas and oceans. Geological Society of America Bulletin 76, 803-832.

Boles, J.R., Franks, S.G., 1979. Clay diagenesis in Wilcox sandstones of Southwest Texas; implications of smectite diagenesis on sandstone cementation. Journal of Sedimentary Research 49, 55-70.

Borges, J.B., Huh, Y., Moon, S., Noh, H., 2008. Provenance and weathering control on river bed sediments of the eastern Tibetan Plateau and the Russian Far East. Chemical Geology 254, 52-72.

Bouchez, J., Gaillardet, J., France-Lanord, C., Maurice, L., Dutra-Maia, P., 2011. Grain size control of river suspended sediment geochemistry: Clues from Amazon River depth profiles. Geochemistry, Geophysics, Geosystems 12, https://doi.org/10.1029/2010GC003380

Bouchez, J., Gaillardet, J., Lupker, M., Louvat, P., France-Lanord, C., Maurice, L., Armijos, E., Moquet, J.S., 2012. Floodplains of large rivers: Weathering reactors or simple silos? Chemical Geology 332, 166-184.

Bradly, P.V. and Carrol, S.A., 1994. Direct effects of CO2 and temperature on silicate weathering: possible implications for climate control. Geochimica and Cosmochimica Acta 58, 1853-1856.

Buggle, B., Glaser, B., Hambach, U., Gerasimenko, N., Markovic, S., 2011. An evaluation of geochemical weathering indices in loess-paleosol studies. Quaternary International 240, 12-21.

Burke, K., Gunnell, Y., 2008. The African erosion surface: a continental-scale synthesis of geomorphology, tectonics, and environmental change over the past 180 million years (Vol. 201). Geological Society of America.

Canfield, D.E., 1997. The geochemistry of river particulates from the continental USA: major elements. Geochimica et Cosmochimica Acta 61, 3349-3365.

Carvalho, H., Tassinari, C., Alves, P.H., Guimarães, F., Simões, M.C., 2000. Geochronological review of the Precambrian in western Angola: links with Brazil. Journal of African Earth Sciences 31, 383-402.

Chaboureau, A.-C., Guillocheau, F., Robin, C., Rohais, S., Moulin, M., Aslanian, D., 2013. Paleogeographic evolution of the central segment of the South Atlantic during Early Cretaceous times: Paleotopographic and geodynamic implications. Tectonophysics 604, 191–223.

Chermak, J.A., Rimstidt, J.D., 1990. The hydrothermal transformation rate of kaolinite to muscovite/illite. Geochimica et Cosmochimica Acta 54, 2979–2990.

Chetelat, B., Liu, C. Q., Wang, Q., Zhang, G., 2013. Assessing the influence of lithology on weathering indices of Changjiang river sediments. Chemical Geology 359, 108-115.

Clift, P.D., Wan, S., Blusztajn, J., 2014. Reconstructing chemical weathering, physical erosion and monsoon intensity since 25 Ma in the northern South China Sea: a review of competing proxies. Earth-Science Reviews 130, 86-102.

Cole, T.G., Shaw, H.F., 1983. The nature and origin of authigenic smectites in some recent marine sediments. Clay Minerals 18, 239-252.

Contrucci, I., Matias, L., Moulin, M., Géli, L., Klingelhofer, F., Nouzé, H., Aslanian, D., Olivet, J.L., Réhault, J.P., Sibuet, J.C., 2004. Deep structure of the West African continental margin (Congo, Zaïre, Angola), between 5°S and 8°S, from reflection/refraction seismics and gravity data. Geophysical Journal International 158, 529-553.

Crosby, A. G., Fishwick, S., & White, N., 2010. Structure and evolution of the intracratonic Congo Basin. Geochemistry, Geophysics, Geosystems 11, https://doi.org/10.1029/2009GC003014

Daly, M.C., Lawrence, S. R., Diemu-Tshiband, K., Matouana, B., 1992. Tectonic evolution of the Cuvette Centrale, Zaire. Journal of the Geological Society 149, 539-546.

Dellinger, M., Gaillardet, J., Bouchez, J., Calmels, D., Galy, V., Hilton, R.G., Louvat, P, France-Lanord, C., 2014. Lithium isotopes in large rivers reveal the cannibalistic nature of modern continental weathering and erosion. Earth and Planetary Science Letters 401, 359-372.

de Waele, B., Johnson, S.P., Pisarevsky, S.A., 2008. Palaeoproterozoic to Neoproterozoic growth and evolution of the eastern Congo Craton: its role in the Rodinia puzzle. Precambrian Research 160, 127-141.

Deconinck, J.F., Hesselbo, S.P., Debuisser, N., Averbuch, O., Baudin, F., Bessa, J., 2003. Environmental controls on clay mineralogy of an Early Jurassic mudrock (Blue Lias Formation, southern England). International Journal of Earth Sciences 92, 255–266.

Dessert, C., Dupré, B., Gaillardet, J., François, L. M., Allegre, C.J., 2003. Basalt weathering laws and the impact of basalt weathering on the global carbon cycle. Chemical Geology 202, 257-273.

Diefendorf, A.F., Mueller, K.E., Wing, S.L., Koch, P.L., Freeman, K.H., 2010. Global patterns in leaf 13C discrimination and implications for studies of past and future climate. Proceedings of the National Academy of Sciences 107, 5738-5743.

Dinis, P., Oliveira, Á., 2016. Provenance of Pliocene clay deposits from the Iberian Atlantic Margin and compositional changes during recycling. Sedimentary Geology 336, 171-182.

Dinis, P., Garzanti, E., Vermeesch, P., Huvi, J., 2017. Climatic zonation and weathering control on sediment composition (Angola). Chemical Geology 467, 110-121.

Dupré, B., Dessert, C., Oliva, P., Goddéris, Y., Viers, J., François, L., Millot, R., Gaillardet, J., 2003. Rivers, chemical weathering and Earth's climate. Comptes Rendus Geoscience 335, 1141-1160.

Dupré, B., Gaillardet, J., Rousseau, D., Allègre, C.J., 1996. Major and trace elements of river-borne material: The Congo Basin. Geochimica et Cosmochimica Acta, 60, 1301-1321.

Ehrmann, W., 1998. Implications of late Eocene to early Miocene clay mineral assemblages in McMurdo Sound (Ross Sea, Antarctica) on paleoclimate and ice dynamics. Palaeogeography, Palaeoclimatology, Palaeoecology 139, 213-231.

Ernst, R.E., Pereira, E., Hamilton, M.A., Pisarevsky, S.A., Rodriques, J., Tassinari, C.C., Teixeira, W., Van-Dunem, V., 2013. Mesoproterozoic intraplate magmatic 'barcode'record of the Angola portion of the Congo Craton: Newly dated magmatic events at 1505 and 1110 Ma and implications for Nuna (Columbia) supercontinent reconstructions. Precambrian Research 230, 103-118.

Fedo, C.M., Nesbitt, H. W., Young, G.M., 1995. Unraveling the effects of potassium metasomatism in sedimentary rocks and paleosols, with implications for paleoweathering conditions and provenance. Geology 23, 921-924.

Fernandez-Alonso, M. et al., 2015. Carte Géologique de la République Démocratique du Congo. République Démocratique du Congo, Ministère des Mines.

Fick, S.E. and Hijmans, R.J., 2017. Worldclim 2: New 1-km spatial resolution climate surfaces for global land areas. International Journal of Climatology 37, 4302-4315.

Gabet, E. J., Mudd, S. M., 2009. A theoretical model coupling chemical weathering rates with denudation rates. Geology 37, 151-154.

Gaillardet, J., Dupré, B., Allègre, C.J., 1999. Geochemistry of large river suspended sediments: silicate weathering or recycling tracer? Geochimica et Cosmochimica Acta 63, 4037-4051.

Gallet, S., Jahn, B.M., Lanoë, B.V.V., Dia, A., Rossello, E., 1998. Loess geochemistry and its implications for particle origin and composition of the upper continental crust. Earth and Planetary Science Letters 156, 157-172.

Galy, A., France-Lanord, C., 1999. Weathering processes in the Ganges–Brahmaputra basin and the riverine alkalinity budget. Chemical Geology 159, 31-60.

Galy, V., France-Lanord, C., Lartiges, B., 2008. Loading and fate of particulate organic carbon from the Himalaya to the Ganga–Brahmaputra delta. Geochimica et Cosmochimica Acta 72, 1767-1787.

Garrels, R.M., 1983. The carbonate-silicate geochemical cycle and its effect on atmospheric carbon dioxide over the past 100 million years. American Journal of Science 283, 641-683.

Garzanti E., 2017. The maturity myth in sedimentology and provenance analysis. Journal of Sedimentary Research, 87, 353-365.

Garzanti, E., Andó, S., France-Lanord, C., Censi, P., Vignola, P., Galy, V., Lupker, M., 2011. Mineralogical and chemical variability of fluvial sediments 2. Suspended-load silt (Ganga–Brahmaputra, Bangladesh). Earth and Planetary Science Letters 302, 107-120.

Garzanti, E., Andó, S., Vezzoli G., 2009. Grain-size dependence of sediment composition and environmental bias in provenance studies. Earth and Planetary Science Letters 277, 422-432.

Garzanti, E., Padoan, M., Setti, M., López-Galindo, A., & Villa, I. M., 2014. Provenance versus weathering control on the composition of tropical river mud (southern Africa). Chemical Geology, 366, 61-74.

Garzanti, E., Padoan, M., Setti, M., Peruta, L., Najman, Y., Villa, I.M., 2013. Weathering geochemistry and Sr-Nd isotope fingerprinting of equatorial upper Nile and Congo muds. Geochemistry, Geophysics, Geosystems 14, 292-316.

Garzanti, E., Resentini, A., 2016. Provenance control on chemical indices of weathering (Taiwan river sands). Sedimentary geology 336, 81-95.

Garzanti, E., Dinis, P., Vermeesch, P., Andò, S., Hahn, A., Huvi, J., Limonta, M., Padoan, M., Resentini, A., Rittner, M., Vezzoli, G., 2018a. Sedimentary processes controlling ultralong cells of littoral transport: Placer formation and termination of the Orange sand highway in southern Angola. Sedimentology 65, 431-460.

Garzanti, E., Dinis, P., Vermeesch, P., Andò, S., Hahn, A., Huvi, J., Limonta, M., Padoan, M., Resentini, A., Rittner, M., Vezzoli, G., 2018b. Dynamic uplift, recycling, and climate control on the petrology of passive-margin sand (Angola). Sedimentary Geology 375, 86-104.

Garzanti, E., Vermeesch, P., Andó, S., Limonta, M., Vezzoli G., Dinis, P., Hahn, A., Baudet, D., de Grave, J., Yaya, N.K., 2019. Congo river sand and the equatorial quartz factory. Earth-Science Reviews (this volume).

Gibbs, R.J., 1977. Clay mineral segregation in the marine environment. Journal of Sedimentary Research 47, 237-243.

Giresse, P., 2005. Mesozoic–Cenozoic history of the Congo basin. Journal of African Earth Sciences 43, 301-315.

Govin, A., Holzwarth, U., Heslop, D., Ford Keeling, L., Zabel, M., Mulitza, S., Collins, J.A, Chiessi, C.M., 2012. Distribution of major elements in Atlantic surface sediments (36°N–49°S): Imprint of terrigenous input and continental weathering. Geochemistry, Geophysics, Geosystems 13, Q01013. doi:10.1029/2011GC003785

Griffin, J.J., Windom, H., Goldberg, E.D., 1968. The distribution of clay minerals in the world ocean. In Deep Sea Research and Oceanographic 15, 433-459.

Grimes, S.T., Collinson, M.E., Hooker, J.J., Mattey, D.P., 2008. Is small beautiful? A review of the advantages and limitations of using small mammal teeth and the direct laser fluorination analysis technique in the isotope reconstruction of past continental climate change. Palaeogeography, Palaeoclimatology, Palaeoecology 266, 39-50.

Gu, X.X., Liu, J.M., Zheng, M. H., Tang, J. X., Qi, L., 2002. Provenance and tectonic setting of the Proterozoic turbidites in Hunan. South China: geochemical evidence. Journal of Sedimentary Research 72, 393–407.

Guillocheau, F., Simon, B., Baby, G., Bessin, P., Robin, C., Dauteuil, O., 2018. Planation surfaces as a record of mantle dynamics: The case example of Africa. Gondwana Research, 53, 82–98.

Guiraud, M., Buta-Neto, A., & Quesne, D., 2010. Segmentation and differential post-rift uplift at the Angola margin as recorded by the transform-rifted Benguela and oblique-to-orthogonal-rifted Kwanza basins. Marine and Petroleum Geology 27, 1040-1068.

Guo, Y., Yang, S., Su, N., Li, C., Yin, P., Wang, Z., 2018. Revisiting the effects of hydrodynamic sorting and sedimentary recycling on chemical weathering indices. Geochimica et Cosmochimica Acta 227, 48-63.

Haddon, I.G., McCarthy, T.S., 2005. The Mesozoic–Cenozoic interior sag basins of Central Africa: The Late-Cretaceous–Cenozoic Kalahari and Okavango basins. Journal of African Earth Sciences 43, 316-333.

Harnois, L., 1988. The CIW index: a new chemical index of weathering. Sedimentary geology, 55 319-322.

Heilborn, M., Valeriano, C.M., Tassinari, C.C.G., Almeida, J., Tupinambá, M., Siga Jr, O., Trouw, R., 2008. Correlation of Neoproterozoic terranes between the Ribeira Belt, SE Brazil and its African counterpart: comparative tectonic evolution and open questions. In: Pankhurst, R. J., Trouw, R. A. J., Brito Neves, B.B., Wit, M.J. (Eds.), West Gondwana: Pre-Cenozoic Correlations Across the South Atlantic Region. Geological Society, London, Spec. Publ. 294, pp. 211–237.

Hessler, A.M., Zhang, J., Covault, J., Ambrose, W., 2017. Continental weathering coupled to Paleogene climate changes in North America. Geology 45, 911-914.

Hodell, D.A., Brenner, M., Kanfoush, S.L., Curtis, J.H., Stoner, J.S., Xueliang, S., Yuan, W., Whitmore, T.J., 1999. Paleoclimate of southwestern China for the past 50,000 yr inferred from lake sediment records. Quaternary Research 52, 369-380.

Hong, H., Li, Z., Xue, H., Zhu, Y., Zhang, K., Xiang, S., 2007. Oligocene clay mineralogy of the Linxia Basin: evidence of paleoclimatic evolution subsequent to the initial-stage uplift of the Tibetan Plateau. Clays and Clay Minerals 55, 491-503.

Hower, J., Eslinger, E.G., Hower, M.E., Perry, E.A., 1976. Mechanism of burial metamorphism of argillaceous sediment: 1. Mineralogical and chemical evidence. Geological Society of America Bulletin 87, 725–737.

Hu, Z., Gao, S., 2008. Upper crustal abundances of trace elements: a revision and update. Chemical Geology 253, 205-221.

Hundert, T., Piper, D.J.W., Pe-Piper, G., 2006. Genetic model and exploration guidelines for kaolin beneath unconformities in the Lower Cretaceous fluvial Chaswood Formation, Nova Scotia. Exploration and Mining Geology 15, 9-26.

Jackson, M.P.A, Hudec, M.R., Hegarty, K.A., 2005. The great West African Tertiary coastal uplift: fact or fiction? A perspective from the Angolan divergent margin. Tectonics, 24, TC6014, doi:10.1029/2005TC001836.

Jansen, N., Hartmann, J., Lauerwald, R., Dürr, H.H., Kempe, S., Loos, S., Middelkoop, H., 2010. Dissolved silica mobilization in the conterminous USA. Chemical Geology 270, 90-109.

Johnsson, M.J. and Meade, R.H., 1990. Chemical weathering of fluvial sediments during alluvial storage: The Macuapanim Island point bar, Solim6es River, Brazil. Journal of Sedimentary Petrology, 60, 827-842.

Kadima, E., Delvaux, D., Sebagenzi, S.N., Tack, L., Kabeya, S.M., 2011. Structure and geological history of the Congo Basin: an integrated interpretation of gravity, magnetic and reflection seismic data. Basin Research 23, 499-527.

Kahle, M., Kleber, M., Jahn, R., 2002. Review of XRD-based quantitative analyses of clay minerals in soils: the suitability of mineral intensity factors. Geoderma 109, 191-205.

Kalm, V.E., Rutter, N.W., Rokosh, C.D., 1996. Clay minerals and their paleoenvironmental interpretation in the Baoji loess section, Southern Loess Plateau, China. Catena 27, 49-61.

Klingebiel, A., 1963. Observations sur la sédimentation argileuse du début des temps tertiaires en Aquitaine. Bulletin de la Société Géologique de France 7, 303-306.

Köhn, M., 1928. Bemerkungen zur mechanischen Bodenanalyse. III. Ein neuer Pipettapparat. Zeitschrift für Pflanzenernährung, Düngung, Bodenkunde 11, 50-54.

Kump, L.R., Brantley, S.L., Arthur, M.A., 2000. Chemical weathering, atmospheric CO2, and climate. Annual Review of Earth and Planetary Sciences 28, 611-667.

Leng, M.J., Marshall, J.D., 2004. Palaeoclimate interpretation of stable isotope data from lake sediment archives. Quaternary Science Reviews 23, 811-831.

Liu, J., Chen, J., Selvaraj, K., Xu, Q., Wang, Z., Chen, F., 2014. Chemical weathering over the last 1200 years recorded in the sediments of Gonghai Lake, Lvliang Mountains, North China: a high-resolution proxy of past climate. Boreas 43, 914-923.

Louvat, P., Gislason, S.R., Allègre, C.J., 2008. Chemical and mechanical erosion rates in Iceland as deduced from river dissolved and solid material. American Journal of Science 308, 679-726.

Marzoli, A., Melluso, L., Morra, V., Renne, P.R., Sgrosso, I., D'Antonio, M., Duarte, L., Morais, E.A.A., Ricci, G., 1999. Geochronology and petrology of Cretaceous basaltic magmatism in the Kwanza basin (western Angola), and relationship with the Paranà-Etendeka continental flood basalt province. Journal of Geodynamics 28, 341-356.

Mayer, A., Hofmann, A.W., Sinigoi, S., Morais, E., 2004. Mesoproterozoic Sm–Nd and U–Pb ages for the Kunene anorthosite complex of SW Angola. Precambrian Research 133, 187-206.

Maynard, J.B., 1992. Chemistry of modern soils as a guide to interpreting Precambrian paleosols. The Journal of Geology 100, 279-289.

Michalopoulos, P., Aller, R.C., 1995. Rapid clay mineral formation in Amazon delta sediments: reverse weathering and oceanic elemental cycles. Science 270, 614–617.

Minasny, B., Finke, P., Stockmann, U., Vanwalleghem, T., McBratney, A.B., 2015. Resolving the integral connection between pedogenesis and landscape evolution. Earth-Science Reviews 150, 102-120.

McDermott, F., 2004. Palaeo-climate reconstruction from stable isotope variations in speleothems: a review. Quaternary Science Reviews 23, 901-918.

Meunier, A., Caner, L., Hubert, F., El Albani, A. and Prêt, D., 2013. The weathering intensity scale (WIS): an alternative approach of the chemical index of alteration (CIA). American journal of science, 313(2), pp.113-143.

Meybeck, M., 1987. Global chemical weathering of surficial rocks estimated from river dissolved loads. American journal of science 287, 401-428.

Moore, D., Reynolds, R., 1997. X-Ray-Diffraction and the identification and analysis of clay minerals. Oxford University Press, New York.

Moquet, J.S., Crave, A., Viers, J., Seyler, P., Armijos, E., Bourrel, L., Chavarri, E., Lagane, C., Laraque, A., Casimiro, W.S.L, Pombosa, R., Noriega, L, Vera, A., Guyot, J.-L., 2011. Chemical weathering and atmospheric/soil CO2 uptake in the Andean and Foreland Amazon basins. Chemical Geology 287, 1-26.

Moulin, M., Aslanian, D., Unternehr, P., 2010. A new starting point for the South and Equatorial Atlantic Ocean. Earth-Science Reviews 98, 1-37.

Nesbitt, H.W., Young, G.M., 1982. Early Proterozoic climates and plate motions inferred from major element chemistry of lutites. Nature 299, 715-717.

Nesbitt, H.W., Young, G.M., 1989. Formation and diagenesis of weathering profiles. The Journal of Geology 97, 129-147.

Parker, A., 1970. An index of weathering for silicate rocks. Geological Magazine, 107, 501-504.

Parra, M., Delmont, P., Ferragne, A., Latouche, C., Pons, J. C., Puechmaille, C., 1985. Origin and evolution of smectites in recent marine sediments of the NE Atlantic. Clay Minerals 20, 335-346.

Peel, M.C., Finlayson, B.L., McMahon, T.A., 2007. Updated world map of the Koppen-Geiger climate classification. Hydrology and Earth System Sciences 11, 1633-1644.

Petschick, R., Kuhn, G., Gingele, F., 1996. Clay mineral distribution in surface sediments of the South Atlantic: sources, transport, and relation to oceanography. Marine Geology 130, 203-229.

Porter, S.C., 2001. Chinese loess record of monsoon climate during the last glacial–interglacial cycle. Earth-Science Reviews 54, 115-128.

Power, P.E., 1969. Clay mineralogy and paleoclimatic significance of some red regoliths and associated rocks in western Colorado. Journal of Sedimentary Research 39, 876-890

Riebe, C.S., Kirchner, J.W., Finkel, R.C., 2004. Erosional and climatic effects on long-term chemical weathering rates in granitic landscapes spanning diverse climate regimes. Earth and Planetary Science Letters 224, 547-562.

Rieu, R., Allen, P. A., Plotze, M., & Pettke, T., 2007. Compositional and mineralogical variations in a Neoproterozoic glacially influenced succession, Mirbat area, south

Oman: Implications for paleoweathering conditions. Precambrian Research 154, 248-265.

Rimstidt, J.D., Chermak, J.A., Schreiber, M.E., 2017. Processes that control mineral and element abundances in shales. Earth-Science Reviews 171, 383-399.

Rouse, H., 1937. Modern conceptions of the mechanics of fluid turbulence. Transactions of the American Society of Civil Engineers 102, 463–543.

Roy, P.D., Caballero, M., Lozano, R., Smykatz-Kloss, W., 2008. Geochemistry of late Quaternary sediments from Tecocomulco lake, central Mexico: Implication to chemical weathering and provenance. Chem. Erde Geochem. 68, 383–393.

Royer, A., Lécuyer, C., Montuire, S., Amiot, R., Legendre, S., Cuenca-Bescós, G., Jeannet, M., Martineau, F., 2013. What does the oxygen isotope composition of rodent teeth record? Earth and Planetary Science Letters 361, 258-271.

Rudnick, R.L., Gao, S., 2003. Composition of the continental crust. In. R.L Rudnick, H.D. Holland and K.K. Turekian (Eds.) Treatise on geochemistry, 3, The Crust. Elsevier Pergamon, Oxford, 1-64.

Rufyikiri, G., Nootens, D., Dufey, J.E., Delvaux, B., 2004. Mobilization of aluminium and magnesium by roots of banana (Musa spp.) from kaolinite and smectite clay minerals. Applied Geochemistry 19, 633-643.

Sardans, J., Penuelas, J., Ogaya, R., 2008. Drought’s impact on Ca, Fe, Mg, Mo and S concentration and accumulation patterns in the plants and soil of a Mediterranean evergreen Quercus ilex forest. Biogeochemistry 87, 49-69.

Schatz, A.K., Scholten, T., Kühn, P., 2015. Paleoclimate and weathering of the Tokaj (Hungary) loess–paleosol sequence. Palaeogeography, Palaeoclimatology, Palaeoecology 426, 170-182.

Schmitz, B., Andreasson, F.P., 2001. Air humidity and lake δ18O during the latest Paleocene–earliest Eocene in France from recent and fossil fresh-water and marine gastropod δ18O, δ13C, and 87Sr/86Sr. Geological Society of America Bulletin 113, 774-789.

Schulz H., cruise participants, 1992. Bericht und erste Ergebnisse über die METEOR Fahrt M 20-1, Abidjan – Dakar, 131 pp., Berichte, Fachbereich Geowissenschaften, Universität Bremen 25, 173.

Séranne, M., Anka, Z., 2005. South Atlantic continental margins of Africa: a comparison of the tectonic vs climate interplay on the evolution of equatorial west Africa and SW Africa margins. Journal of African Earth Sciences 43, 283-300.

Sheldon, N.D., Tabor, N.J., 2009. Quantitative paleoenvironmental and paleoclimatic reconstruction using paleosols. Earth-science Reviews 95, 1-52.

Šimkevičius, P., Ahlberg, A., Grigelis, A., 2003. Jurassic smectite and kaolinite trends of the East European Platform: implications for palaeobathymetry and palaeoclimate. Terra Nova 15, 225-229.

Singer, A., 1980. The paleoclimatic interpretation of clay minerals in soils and weathering profiles. Earth-Science Reviews 15, 303-326.

Sittler, C., Millot, G., 1964. Les climats du Paléogène français reconstitués par les argiles néoformées et les microflores. Geologische Rundschau 54, 333-343.

Thiry, M., 2000. Palaeoclimatic interpretation of clay minerals in marine deposits: an outlook from the continental origin. Earth-Science Reviews 49, 201-221.

Tack, L., Wingate, M.T.D., Liégeois, J.P., Fernandez-Alonso, M., Deblond, A., 2001. Early Neoproterozoic magmatism (1000–910 Ma) of the Zadinian and Mayumbian Groups (Bas-Congo): onset of Rodinia rifting at the western edge of the Congo craton. Precambrian Research 110, 277-306.

Tréguer, P.J., De La Rocha, C.L., 2013. The world silica cycle. Annual Review of Marine Science 5, 477–501.

Vanoni, V.A., 2006. Sedimentation engineering. Am. Soc. Civ. Eng., Reston: ASCE Manuals and Reports in Engineering Practice, 54. 418 p.

Vaughan, A.P., Pankhurst, R.J., 2008. Tectonic overview of the West Gondwana margin. Gondwana Research 13, 150-162.

Vermeesch, P., Resentini, A. and Garzanti, E., 2016. An R package for statistical provenance analysis. Sedimentary Geology 336, 14-25.

Viers, J., Dupré, B., & Gaillardet, J., 2009. Chemical composition of suspended sediments in World Rivers: New insights from a new database. Science of the total Environment 407, 853-868.

von Eynatten, H., Tolosana-Delgado, R., & Karius, V., 2012. Sediment generation in modern glacial settings: grain-size and source-rock control on sediment composition. Sedimentary Geology 280, 80-92.

von Eynatten, H., Tolosana-Delgado, R., Karius, V., Bachmann, K., Caracciolo, L., 2016. Sediment generation in humid Mediterranean setting: Grain-size and source-rock control on sediment geochemistry and mineralogy (Sila Massif, Calabria). Sedimentary Geology 336, 68-80.

Walker, J.C., Hays, P.B., Kasting, J.F., 1981. A negative feedback mechanism for the long-term stabilization of Earth's surface temperature. Journal of Geophysical Research: Oceans 86(C10), 9776-9782.

Wang, Q.L., Chetelat, B., Zhao, Z.Q., Ding, H., Li, S. L., Wang, B.L., Li, J., Liu, X.L., 2015. Behavior of lithium isotopes in the Changjiang River system: Sources effects and response to weathering and erosion. Geochimica et Cosmochimica Acta 151, 117-132.

Weaver, C.E., 1989. Clays, muds, and shales. Developments in Sedimentology 44. Elsevier.

Wefer, G., cruise participants, 1988. Bericht über METEOR Fahrt M 6-6, Libre Ville – Las Palmas, 97 pp., Berichte, Fachbereich Geowissenschaften, Universität Bremen, No. 3.

West, A.J., Galy, A., Bickle, M., 2005. Tectonic and climatic controls on silicate weathering. Earth and Planetary Science Letters 235, 211-228.

West. A.J., Bickle, M.J., Collins, R., Brasington, J., 2002. Small-catchment perspective on Hymalayan eathering fluxes. Geology 30, 355-358.

White, A.F. and Blum, A.E., 1995. Effects of climate on chemical weathering in watersheds. Geochimica and Cosmochimica Acta 59, 1729-1747.

Wiggs, G.F., Thomas, D.S., Bullard, J.E., Livingstone, I., 1995. Dune mobility and vegetation cover in the southwest Kalahari Desert. Earth Surface Processes and Landforms 20, 515-529.

Yan, Y, Xia, B, Lin, G, Cui, X, Hu X, Yan, P., Zhang, F., 2007. Geochemistry of the sedimentary rocks from the Nanxiong Basin, South China and implications for provenance, paleoenvironment and paleoclimate at the K/T boundary. Sedimentary Geology 197, 127–140.

Yang, S., Jung, H. S., Li, C., 2004. Two unique weathering regimes in the Changjiang and Huanghe drainage basins: geochemical evidence from river sediments. Sedimentary Geology 164, 19-34.

Yang, S.Y., Li, C.X., Yang, D.Y., Li, X.S., 2004. Chemical weathering of the loess deposits in the lower Changjiang Valley, China, and paleoclimatic implications. Quaternary International 117, 27-34.

## Figure captions

Fig. 1: General features of the study area. (A) Location in Southern Africa; the dotted line indicates the areas studied in Petschick et al. (1996) and Garzanti et al. (2013, 2014), whose data are used in the present research. (B) Topography, and location of fluvial and offshore samples in which the geochemistry of two size fractions and clay mineralogy were determined. Numbers for marine samples refer to the GeoB cores. (C) Rainfall (mm) and (D) temperature (°C) in the Congo River basin and along the SW African Atlantic margin (from Fick and Hijmans, 2017).

Fig. 2: Schematic geological map of the SW Africa Atlantic Margin and Congo River basin. Based on CGMW-BRGM (2016). LCB: Lower Congo Basin; KB: Kwanza Basin; NB: Namibe Basin. Drainage basins investigated in this study are outlined.

Fig. 3: Chemical composition of river muds. (A) Ratio between element concentrations in the < 2 µm and < 32 µm fractions, (B) Composition of the two mud fractions in the lower Congo and SW Atlantic margin, (C) Composition of upper Congo (<63 µm fraction) and Namibia (<32 µm fraction) river muds. Element concentrations are

normalized to the UCC and the chemical elements are ranked on the X-axis according to their increasing enrichment relative to the UCC. Dashed lines indicate maximum and minimum values and solid lines indicate average composition.

Fig. 4: Map of the principal components for a selection of chemical elements of the <32 µm (A) and <2 µm (B) fractions. PCA performed with the provenance R-package (Vermeesch et al., 2016). Geochemical data were subjected to a centred log-ratio transformation in order to remove the unit-sum constraint (Aitchison, 1986). The vector loadings of the PCA for the <32 µm fraction define two perpendicular links, indicating two independent controls on the data (Aitchison and Greenacre, 2002). The first link connects the mobile elements (Ca, Na, Al and Ti) and is attributed to weathering (blue). The second link connects elements (Mg, Mn, Co, Th, U, W, LREE) that are linked to source rock geology (brown). These two components are less visible in the fine fraction (<2um).

Fig. 5: Comparison of the levels of depletion/enrichment in different elements relative to the UCC ($\alpha^{Al}_{E}$) in the <2 µm and <32 µm fractions of river muds. (A and B) Average values of $\alpha^{Al}_{E}$ in the <2 µm and <32 µm fractions. Na, followed distantly by Ca and Sr, is the most depleted element. Non-mobile elements may show values higher than 1 where Al concentration is even higher. The size of the circle diameter is proportional to the observed correlation between the <2 µm and <32 µm fractions. The lack of

correlation for CaO is strongly conditioned by the anomalous low Ca content in the Congo Estuary (r=0.92 if this sample is excluded). (C) Levels of depletion in Zr ($\alpha_{Zr}^{Al}$) in muds from different regions. Far better correlations occur if muds collected at different latitudes are isolated.

Fig. 6: Variation with water depth of different compositional features of offshore marine muds. (A) Si/Al and concentration of $TiO_2$ and Zr in the <5 µm fraction. (B) Levels of depletion in Mg ($\alpha^{Al}{}_{Mg}$) and K ($\alpha^{Al}{}_{K}$) and CIA in the <5 µm fraction. (C) Levels of depletion in Mg and K and CIA in the <63 µm fraction.

Fig. 7: Clay mineral assemblages in river muds and marine deposits from Southern Africa (A). Temperate/arid steppe and arid Namibia samples from Garzanti et al. (2014); equatorial upper Congo samples from Garzanti et al. (2013); offshore samples from Petschick et al. (1996). Variation in smectite content in offshore samples with water depth in equatorial (<12.5° latitude; B) and sub-tropical (>12.5° latitude; C)

Fig. 8: Relations between average annual rainfall in the catchment and diverse compositional parameters of river muds from Southern Africa (0-30° latitude). CIA (A),

WIP (B) and the level of depletion in Mg ($\alpha^{Al}_{Mg}$) (C) were obtained for the <32 µm fraction, with the exception of samples from equatorial upper Congo (<63 µm). Kaolinite proportion in the clay assemblage (D) was determined in the <2 µm fraction for all samples. Equatorial upper Congo and temperate/arid steppe and arid Namibia samples from Garzanti et al. (2013, 2014). Samples from upper Congo are neglected in the calculation of regression lines for geochemical data (CIA, WIP and $\alpha^{Al}_{Mg}$).

Fig. 9: Relations between average annual rainfall in the catchment and weathering indices determined from the <2 µm fraction. For geochemical data the dispersion can be reduced if both smaller rivers (drainage area < 2000 $km^2$) and the huge Congo basin are neglected.

Fig. 10: Link between the ratio of Na-depletion in the <2 µm and <32 µm fractions (($\alpha^{Al}_{Na}$)2/ ($\alpha^{Al}_{Na}$)32) and the areal proportion of Meso-Cenozoic sedimentary units in the respective catchments (A). Mucope sand is entirely derived from recycled Kalahari sand. Recycled detritus chiefly consisting of quartz is also overwhelming in Congo and Congo estuary sand and Caculuvar River (Garzanti et al., 2018b and 2019). The large majority of river muds in inset (B) are either from arid to semi-arid settings in coastal southwestern Angola (Curoca, Giraul, Bentiaba, and Carujamba) or from humid settings in northwestern Angola and Bas-Congo draining the West Congo Belt

(Mebridege, Lufu, Lunkunga, Mpozo and Bundi); other sources of recycled material besides Meso-Cenozoic sedimentary units can be considered for these rivers.

## Table captions

Table 1. A selection of compositional parameters that may reflect weathering intensity.

(1) Use molar proportions; (2) Uses monocationic millimoles.

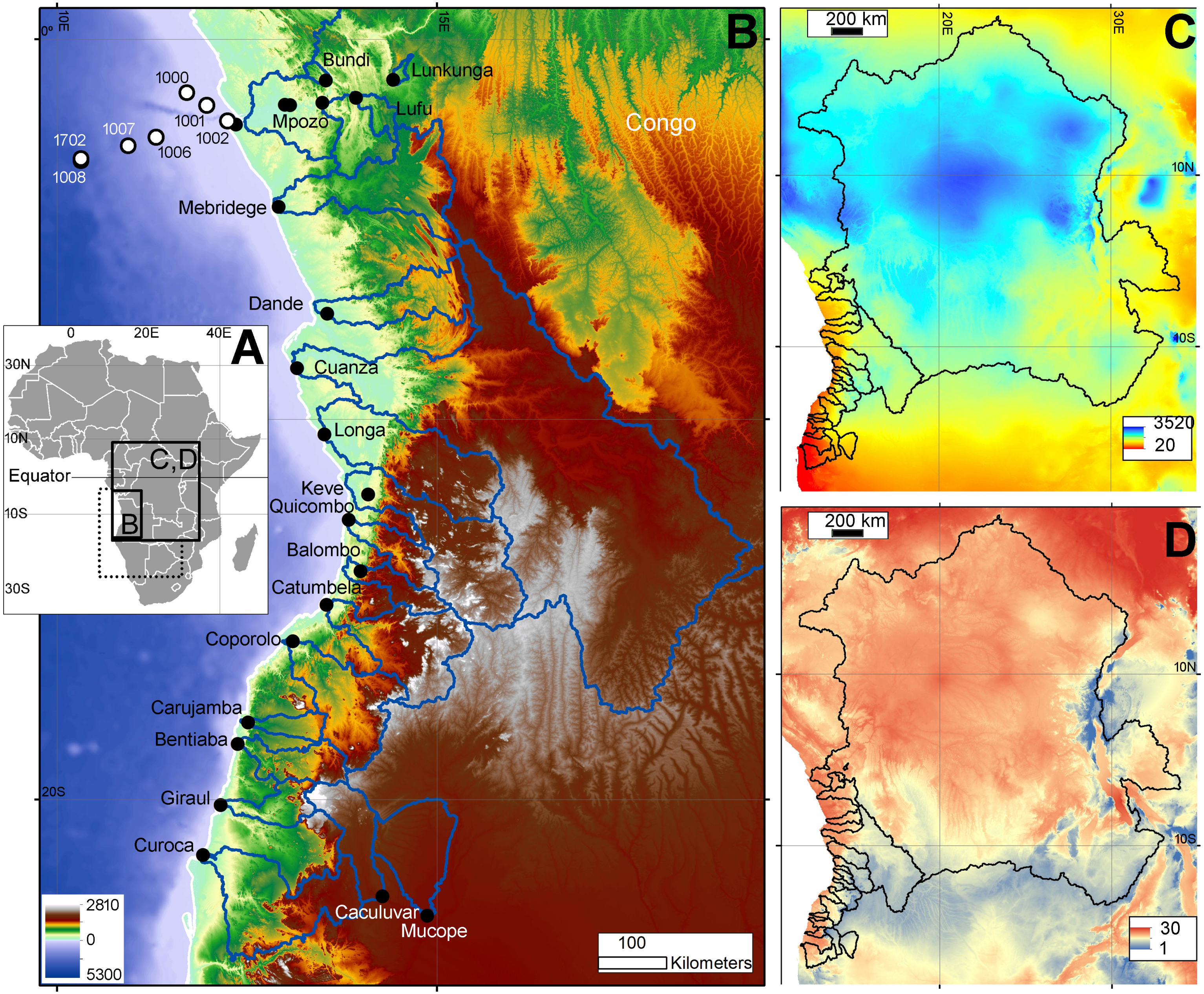

B
10E
15E
0°
20S
Bundi
Lunkunga
Lufu
Mpozo
Congo
1000
1001
1002
1007
1006
1702
1008
Mebridege
Dande
Cuanza
Longa
Keve
Quicombo
Balombo
Catumbela
Coporolo
Carujamba
Bentiaba
Giraul
Curoca
Caculuvar
Mucope
2810
0
5300
100
Kilometers
A
0
20E
40E
30N
10N
Equator
10S
30S
C,D
B
C
200 km
20E
30E
10N
10S
3520
20
D
200 km
10N
10S
30
1

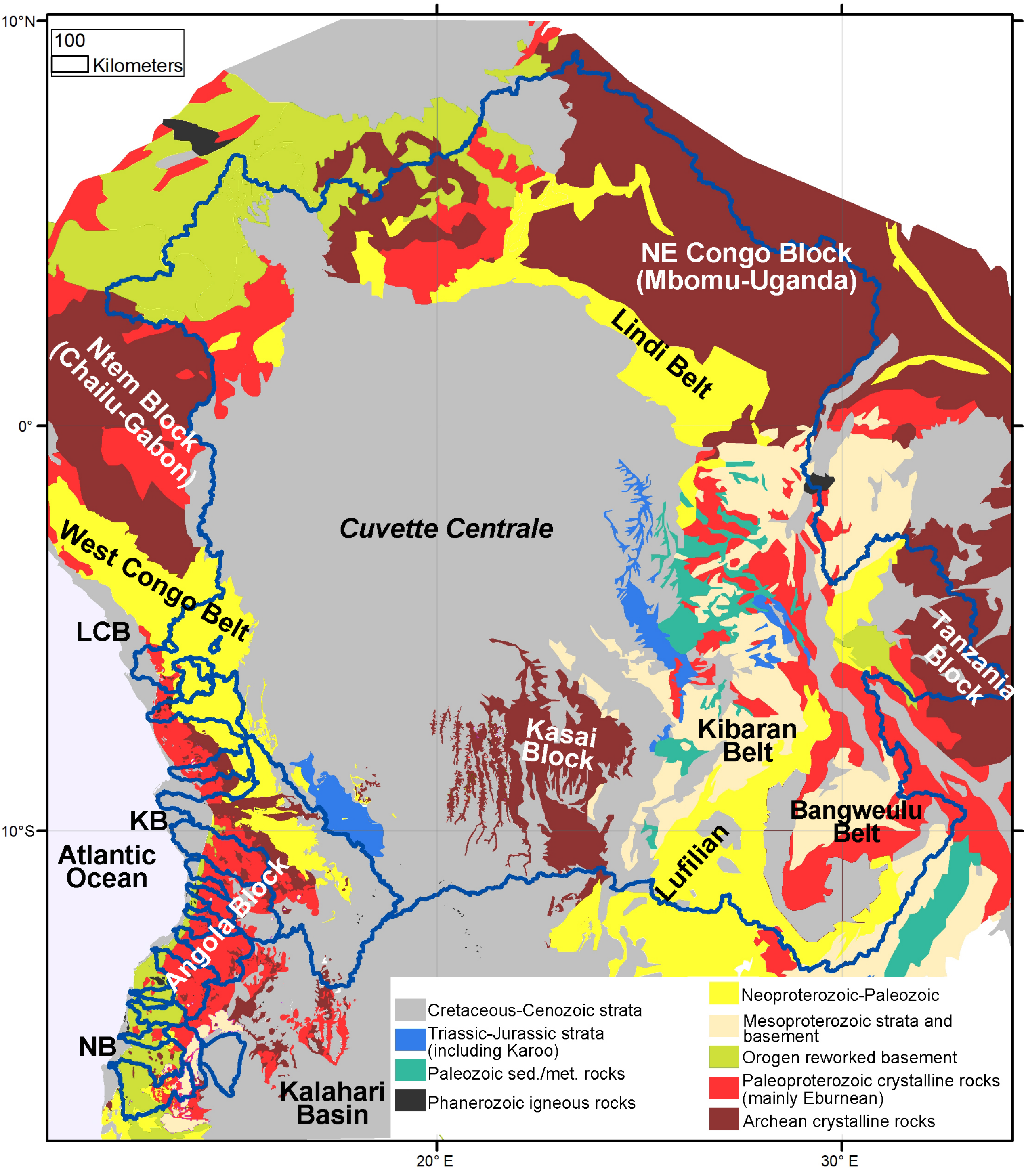
10°N
0°
10°S
20° E
30° E
100
Kilometers
NE Congo Block
(Mbomu-Uganda)
Lindi Belt
Ntem Block
(Chailu-Gabon)
West Congo Belt
LCB
Cuvette Centrale
Tanzania
Block
Kasai
Block
Kibaran
Belt
Bangweulu
Belt
Lufilian
KB
Atlantic
Ocean
Angola Block
NB
Kalahari
Basin
Cretaceous-Cenozoic strata
Triassic-Jurassic strata
(including Karoo)
Paleozoic sed./met. rocks
Phanerozoic igneous rocks
Neoproterozoic-Paleozoic
Mesoproterozoic strata and
basement
Orogen reworked basement
Paleoproterozoic crystalline rocks
(mainly Eburnean)
Archean crystalline rocks

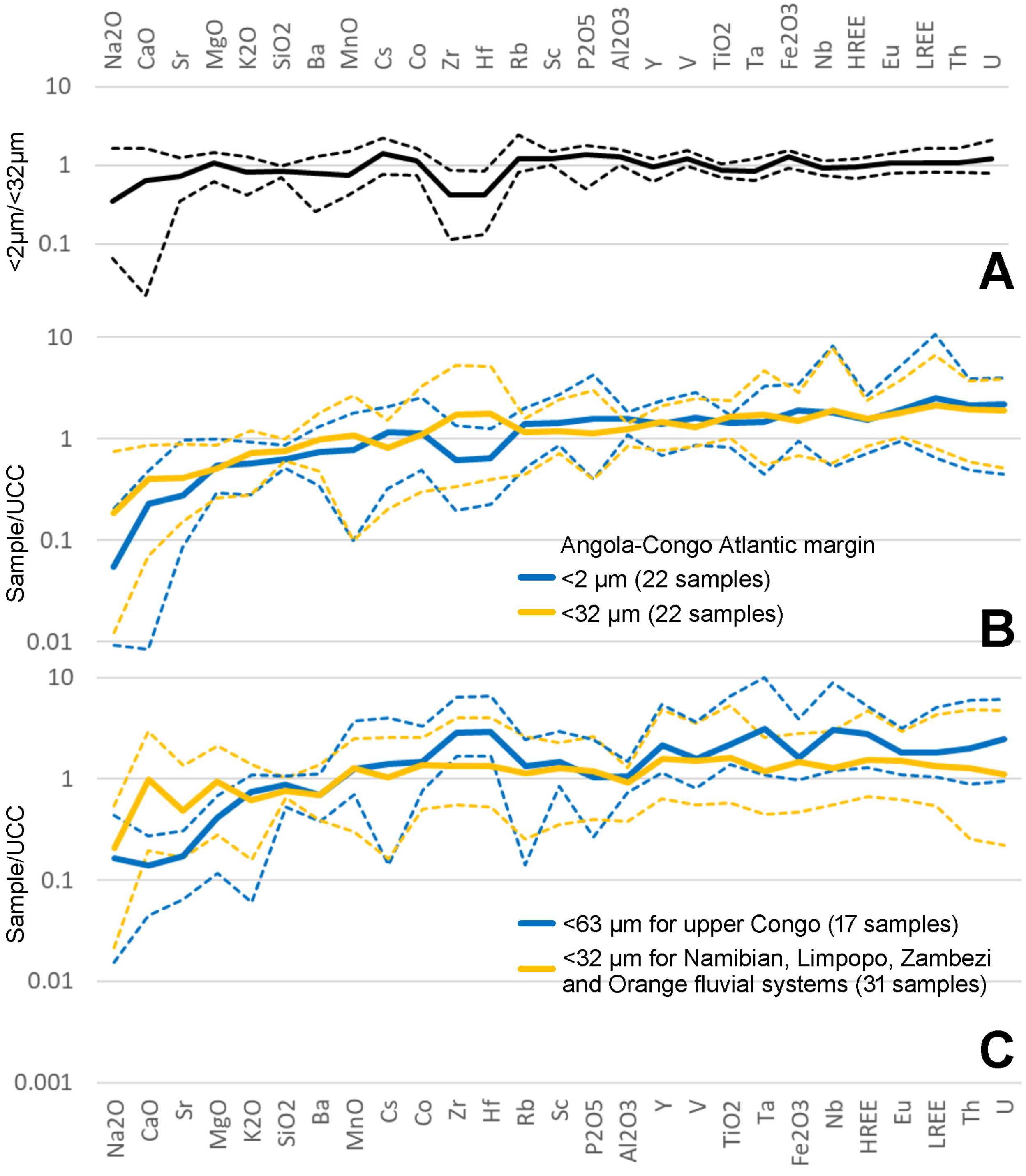

Na2O CaO Sr MgO K2O SiO2 Ba MnO Cs Co Zr Hf Rb Sc P2O5 Al2O3 Y V TiO2 Ta Fe2O3 Nb HREE Eu LREE Th U
10
1
0.1
<2µm/<32µm
A
10
1
0.1
0.01
Sample/UCC
Angola-Congo Atlantic margin
<2 µm (22 samples)
<32 µm (22 samples)
B
10
1
0.1
0.01
0.001
Sample/UCC
<63 µm for upper Congo (17 samples)
<32 µm for Namibian, Limpopo, Zambezi and Orange fluvial systems (31 samples)
C
Na2O CaO Sr MgO K2O SiO2 Ba MnO Cs Co Zr Hf Rb Sc P2O5 Al2O3 Y V TiO2 Ta Fe2O3 Nb HREE Eu LREE Th U

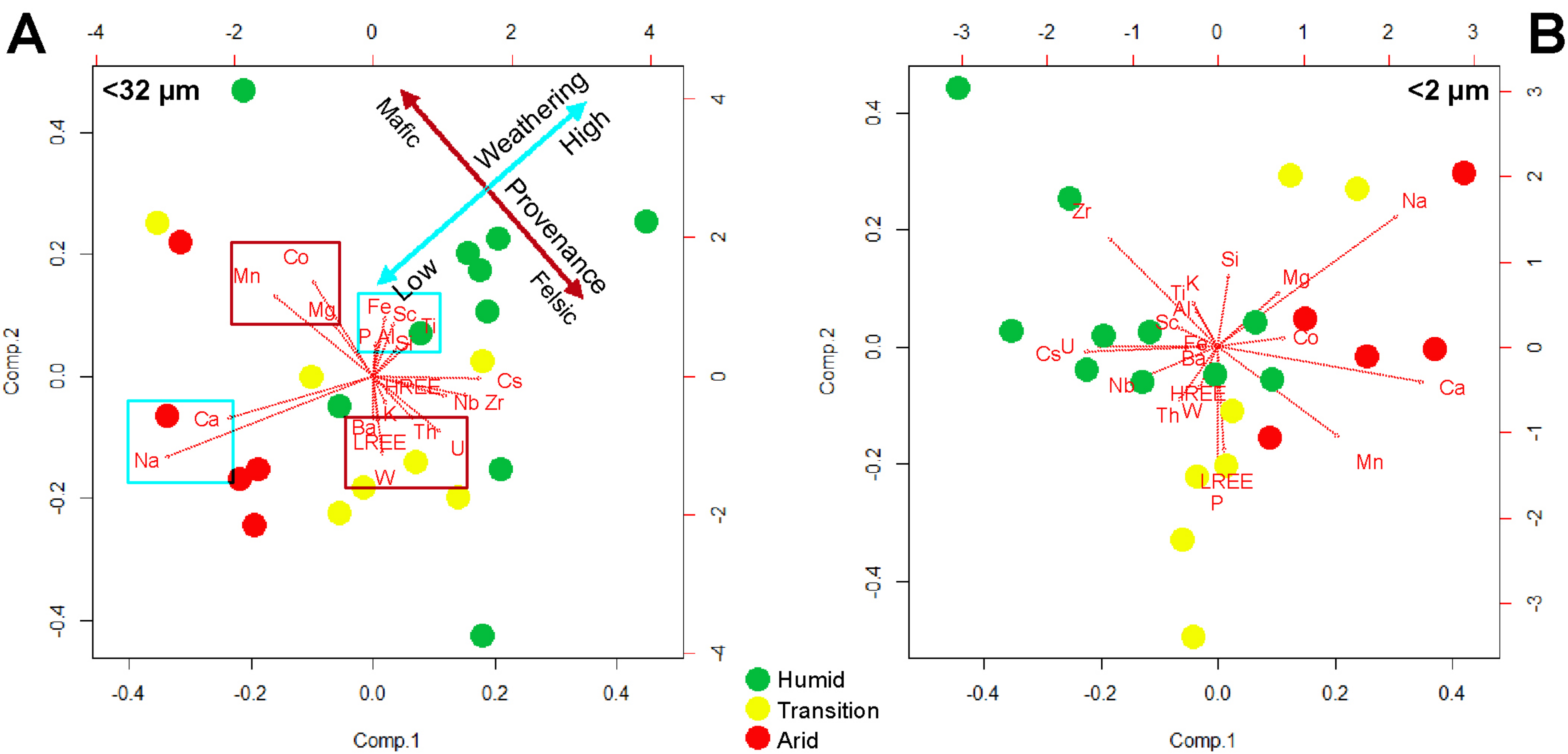

A
<32 µm
Mafic
Weathering
High
Provenance
Low
Felsic
Comp.1
Comp.2
B
<2 µm
Humid
Transition
Arid

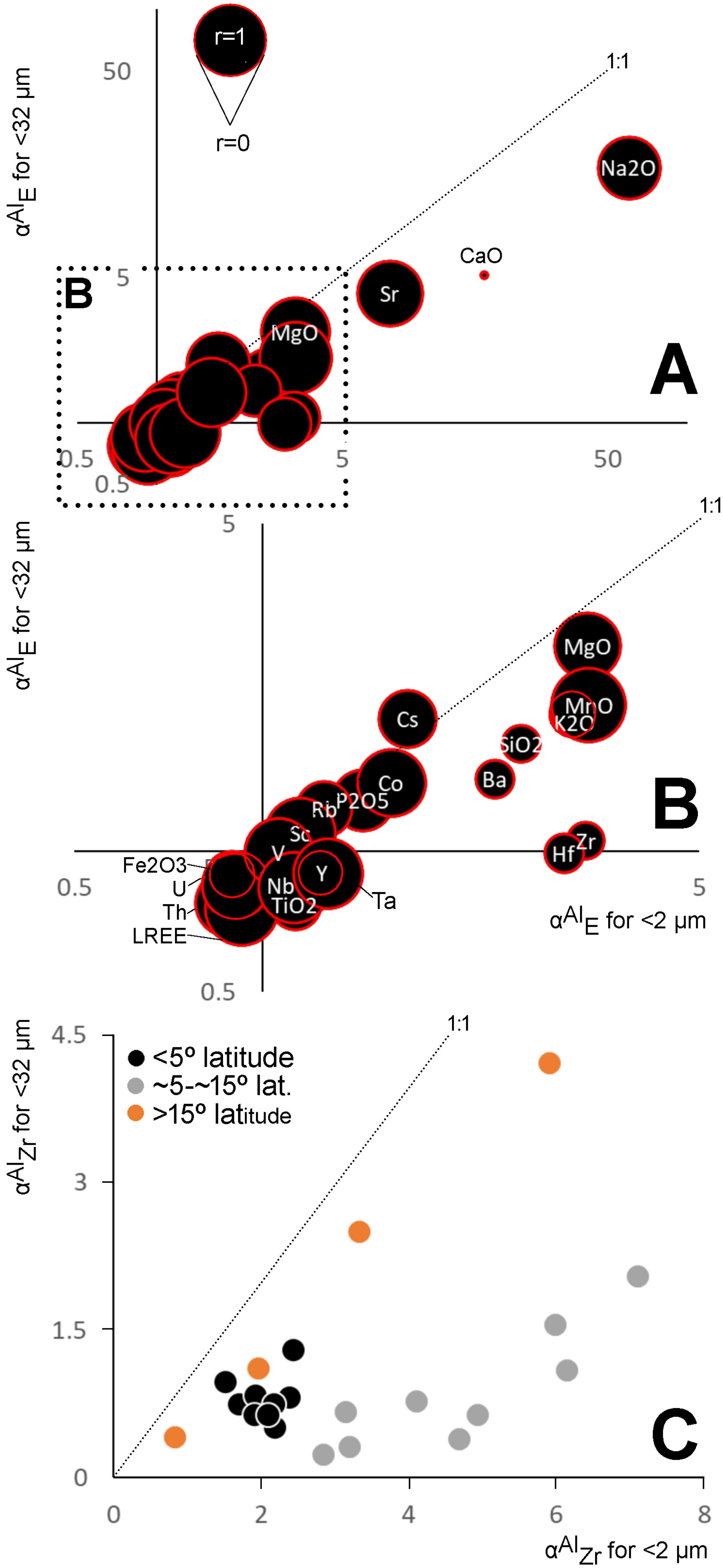

r=1
r=0
1:1
Na2O
CaO
Sr
MgO
A
B
50
5
0.5
αAlE for <32 μm
1:1
MgO
MnO
K2O
Cs
SiO2
Ba
Co
P2O5
Rb
Sc
V
Fe2O3
U
Th
LREE
Nb
TiO2
Y
Ta
Hf
Zr
B
0.5
5
αAlE for <2 μm
αAlE for <32 μm
1:1
<5º latitude
~5-~15º lat.
>15º latitude
C
0
1.5
3
4.5
0
2
4
6
8
αAlZr for <2 μm
αAlZr for <32 μm

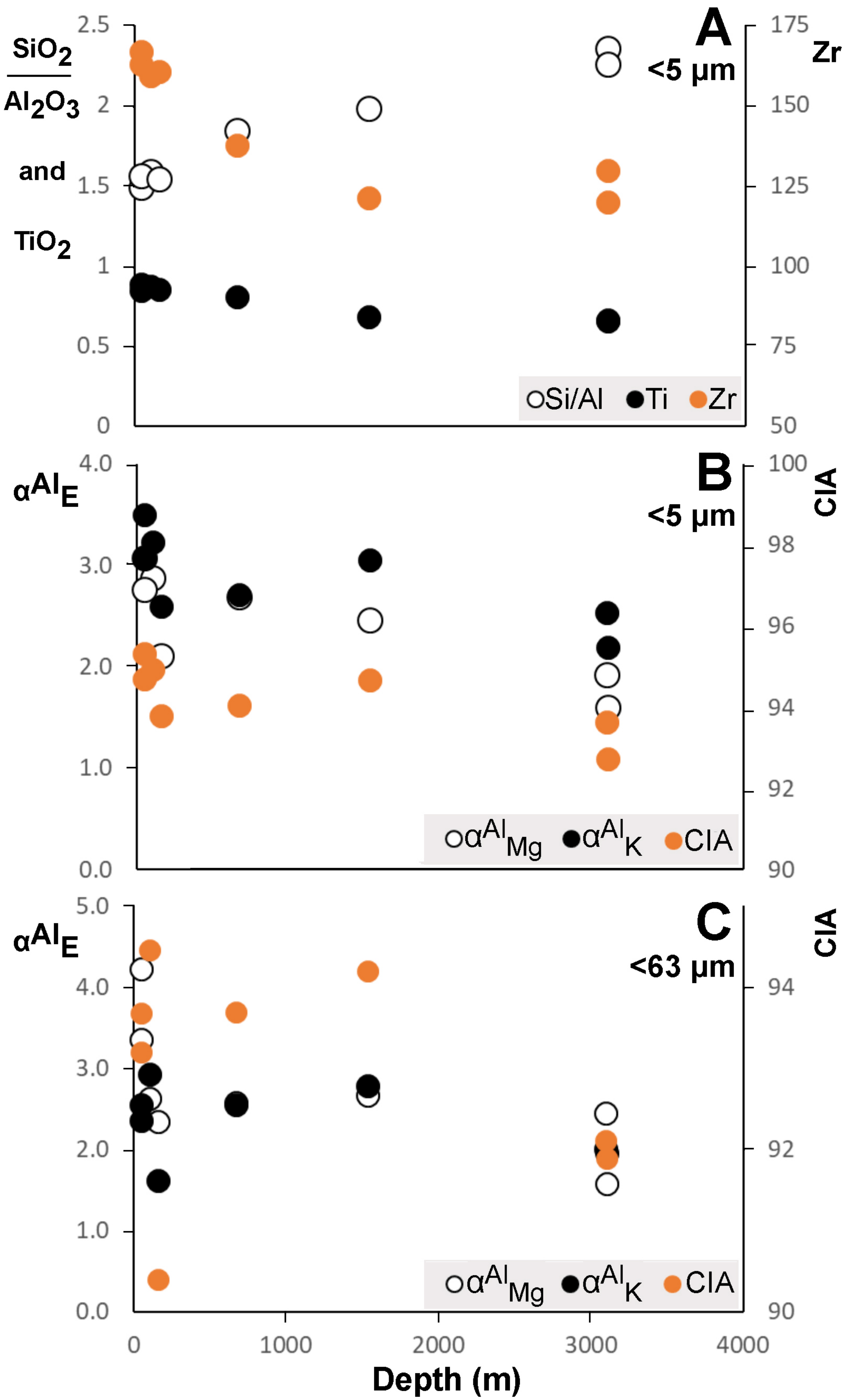

A
<5 µm
SiO2 / Al2O3 and TiO2
Zr
Si/Al
Ti
Zr
B
<5 µm
αAlE
CIA
αAlMg
αAlK
CIA
C
<63 µm
αAlE
CIA
αAlMg
αAlK
CIA
Depth (m)

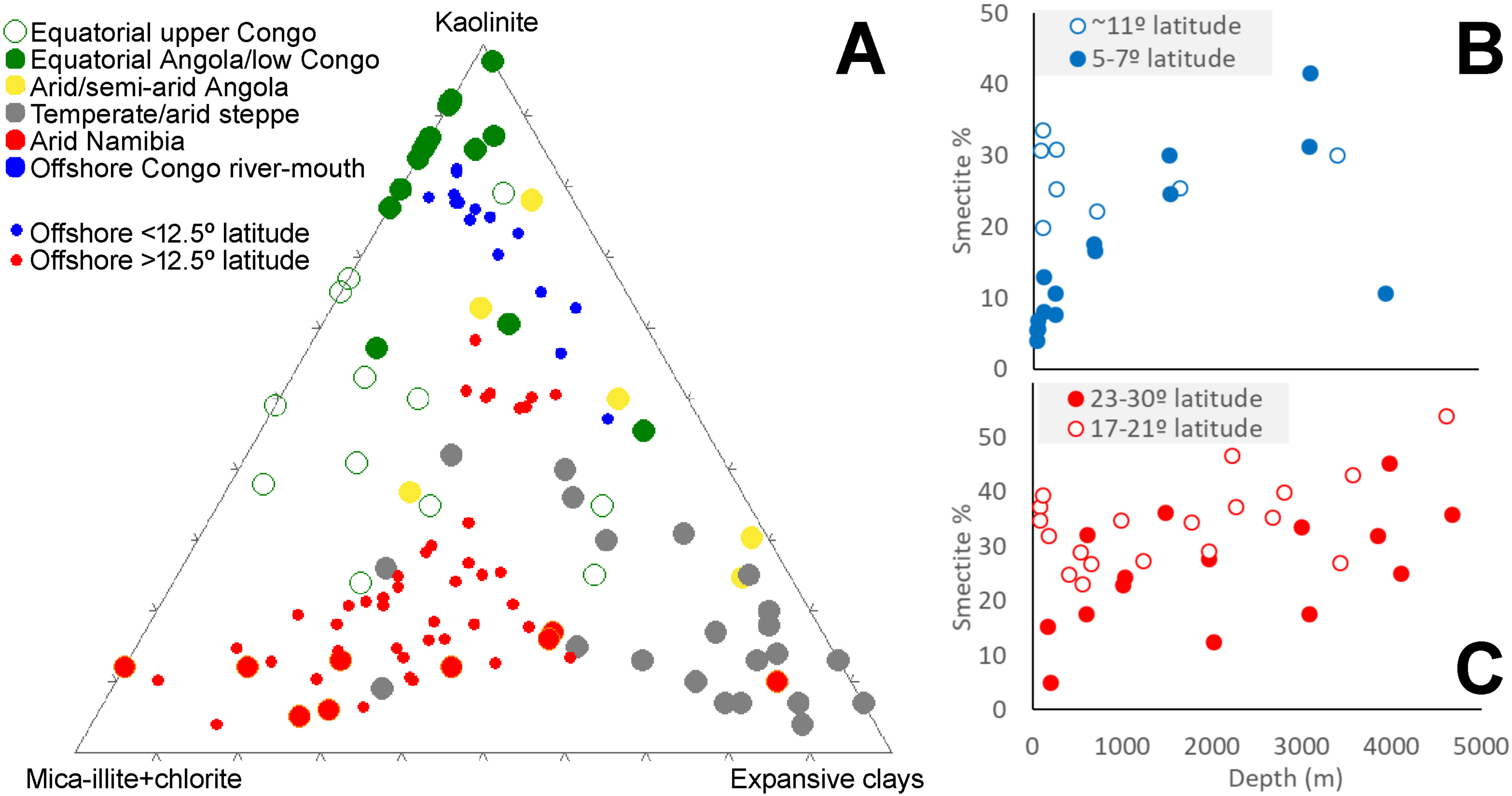

A
Equatorial upper Congo
Equatorial Angola/low Congo
Arid/semi-arid Angola
Temperate/arid steppe
Arid Namibia
Offshore Congo river-mouth
Offshore <12.5º latitude
Offshore >12.5º latitude
Kaolinite
Mica-illite+chlorite
Expansive clays
B
~11º latitude
5-7º latitude
C
23-30º latitude
17-21º latitude
Smectite %
Depth (m)
0
10
20
30
40
50
1000
2000
3000
4000
5000

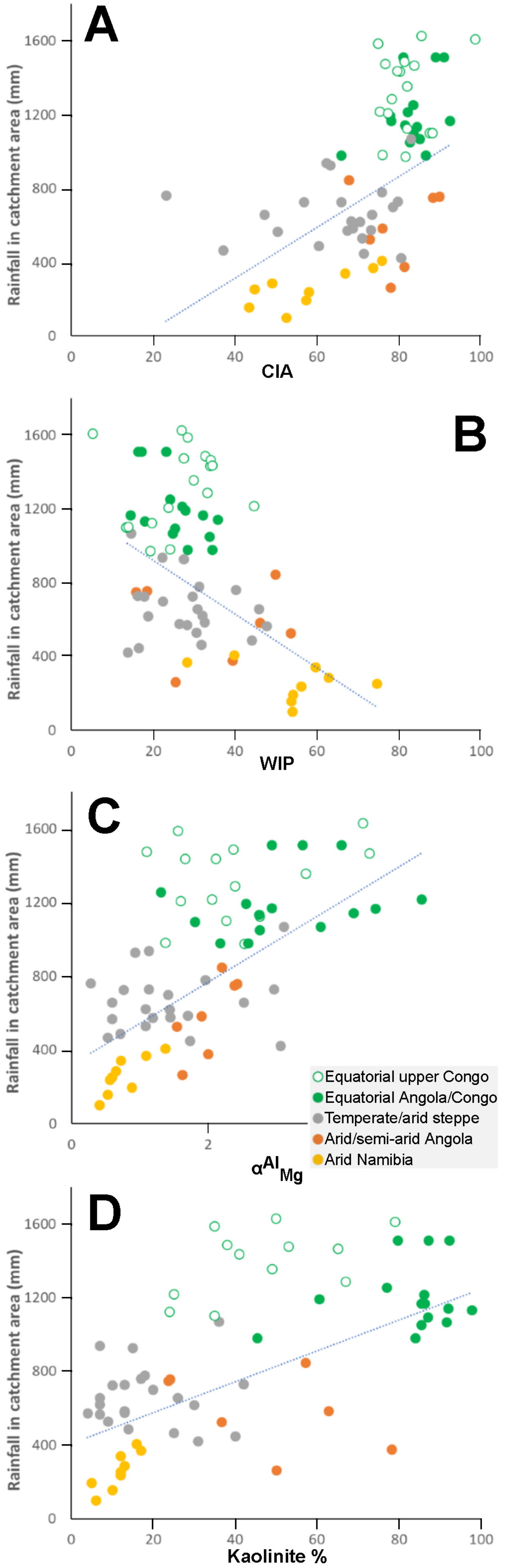

A
B
C
D
Rainfall in catchment area (mm)
CIA
WIP
$\alpha^{Al}_{Mg}$
Kaolinite %
Equatorial upper Congo
Equatorial Angola/Congo
Temperate/arid steppe
Arid/semi-arid Angola
Arid Namibia

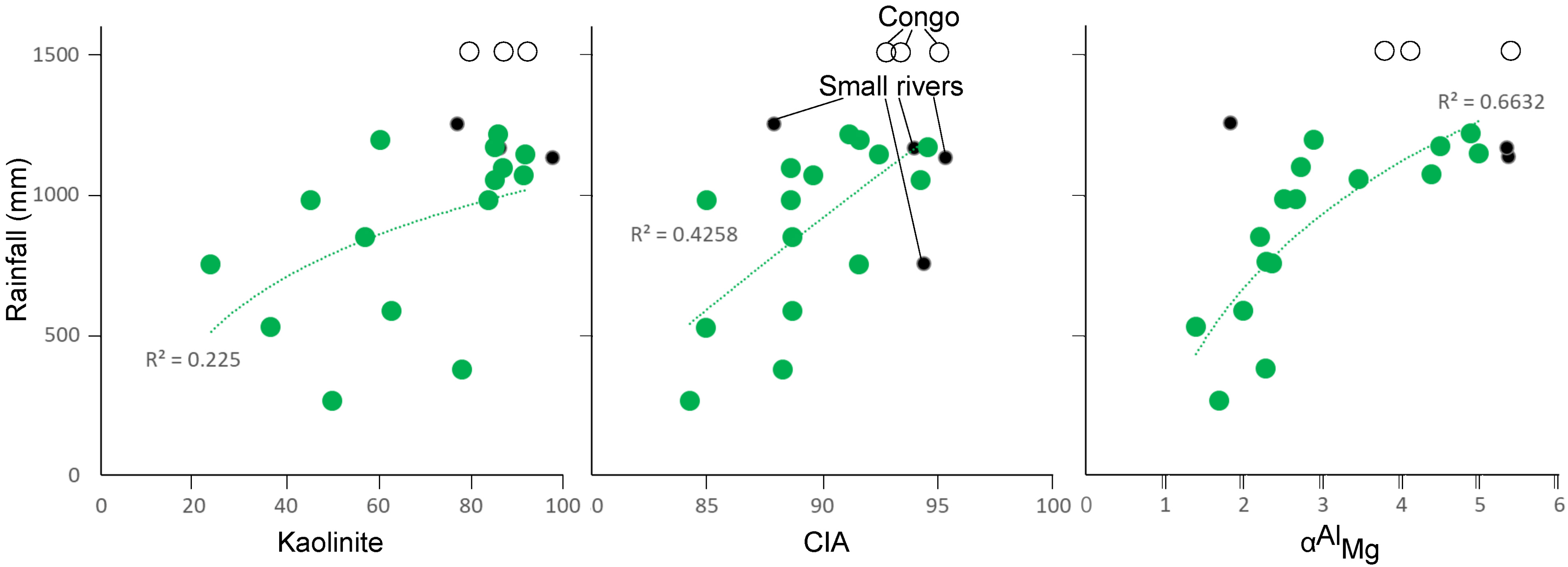
Rainfall (mm)
1500
1000
500
0
0
20
40
60
80
100
Kaolinite
R² = 0.225
Congo
Small rivers
R² = 0.4258
0
85
90
95
100
CIA
R² = 0.6632
0
1
2
3
4
5
6
$\alpha^{Al}_{Mg}$

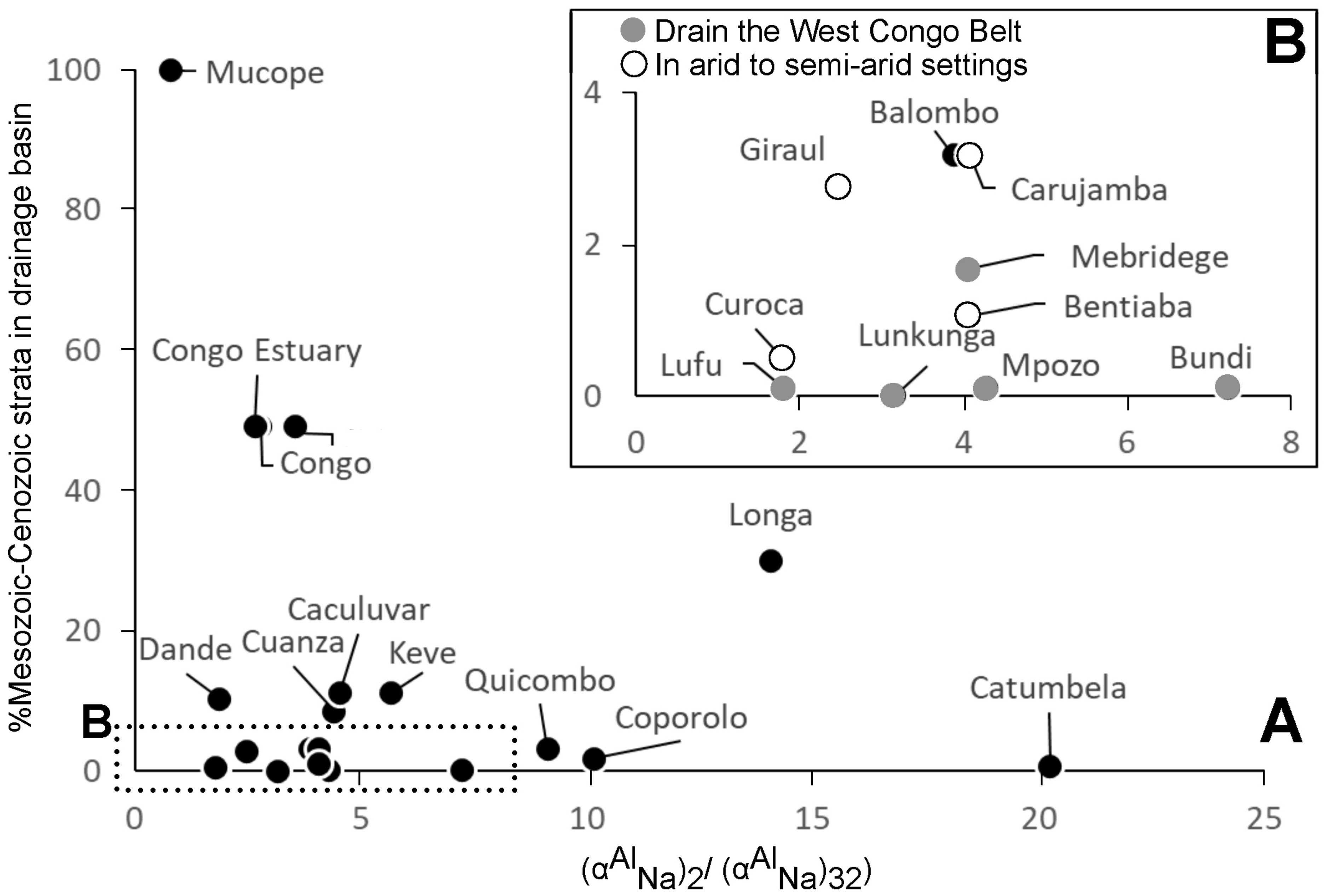

Drain the West Congo Belt
In arid to semi-arid settings
B
Balombo
Giraul
Carujamba
Mebridege
Bentiaba
Curoca
Lunkunga
Lufu
Mpozo
Bundi
Mucope
Congo Estuary
Congo
Longa
Caculuvar
Dande
Cuanza
Keve
Quicombo
Coporolo
Catumbela
B
A
%Mesozoic-Cenozoic strata in drainage basin
$(\alpha^{Al}{}_{Na})_2 / (\alpha^{Al}{}_{Na})_{32}$

Table 1. A selection of compositional parameters that may reflect weathering intensity. (1) Use molar proportions; (2) Uses monocationic millimoles.

| Parameter | Formula (when necessary); Response to weathering | Reference |
|---|---|---|
| Geochemical | | |
| WIP (Weathering Index of Parker) | $(CaO^*/0.7+2Na_2O/0.35+2K_2O/0.25+MgO/0.9)$ X 100 (1); Decreases | Parker (1970) |
| CIA (Chemical Index of Alteration) | $Al_2O_3$ / $(Al_2O_3+K_2O+CaO^*+Na_2O)$ X 100 (1); Increases | Nesbitt and Young (1982) |
| CIW (Chemical Index of Weathering) | $Al_2O_3$ / $(Al_2O3+CaO+Na_2O)$ X 100 (1); Increases | Harnois (1988) |
| PIA (Plagioclase Index of Alteration) | $(Al_2O_3-K_2O)/(Al_2O3+K_2O+Na_2O)$ X 100 (1); Increases | Fedo et al. (1995) |
| Th/U | Increases if Th/U>4 | McLennan et al. (1995), Gu et al. (2002) |
| Th/K | Increases | Deconinck et al (2003) |
| $\alpha_{ME}$ | $(ImE/ME)_{sample}/(ImE/ME)_{UCC}$, being ME a mobile element (Mg, Ca, Na, Sr, K, Ba) and ImE a non-mobile element with similar magmatic compatibility (Al for Mg, Ti for Ca, Sm for Na, Nd for Sr, and Th for K and Ba); Increases | Gaillardet et al. (1999) |
| K/Na and Rb/Sr | Increases | Yang et al. (2004) |
| Cs/Ti and Rb/Ti | Decreases | Yan et al. (2007) |
| W in M-F-W diagram | Long formulation (see cited reference); Progress towards vertex W of M-F-W ternary diagram | Ohta and Arai (2007) |
| Rb/K | Increases | Roy et al. (2008) |
| CPA (Chemical Proxy of Alteration) | $Al_2O_3$ / $(Al_2O3+Na_2O)$ X 100 (1); Increases | Buggle et al. (2011) |
| 4Si in M+-4Si-R2+ diagram | Long formulation (see cited reference) (2); Progress towards vertex 4Si of M+-4Si-R2+ ternary diagram | Meunier et al. (2012) |
| $\alpha^{Al}_{E}$ | $(Al/E)_{sample}/(Al/E)_{UCC}$, being E a mobile elemento; Increases | Garzanti et al. (2013a) |
| $MIA_{(o)}$ (Mafic Index of Alteration for oxidative weathering) | $(Al_2O_3+Fe_2O_3)$ X 100 / $(Al_2O_3+K_2O+CaO^*+Na_2O+MgO)$; Increases | Babechuck et al. (2014) |
| $MIA_{(r)}$ (Mafic Index of Alteration for reductive weathering) | $(Al_2O)$ X 100 / $(Al_2O_3+K_2O+CaO^*+Na_2O+MgO+FeO)$; Increases | Babechuck et al. (2014) |
| CIX (modified CIA) | $Al_2O_3$ / $(Al_2O3+K_2O+Na_2O)$ X 100 (1); Increases | Garzanti et al. (2014) |
| | | |
| Mineralogical | | |
| Kaolinite proportion | Increases | E.g., Chamley (1989), Velde (1996) |
| MIA (Mineralogical Index of Alteration) | Quartz%/(Quartz%+Feldspar%) X 100; Increases | Rieu et al. (2007); Hessler et al. (2017) |